iScience

CellPress
OPEN ACCESS

Article

FAP promotes metastasis and chemoresistance via regulating YAP1 and macrophages in mucinous colorectal adenocarcinoma

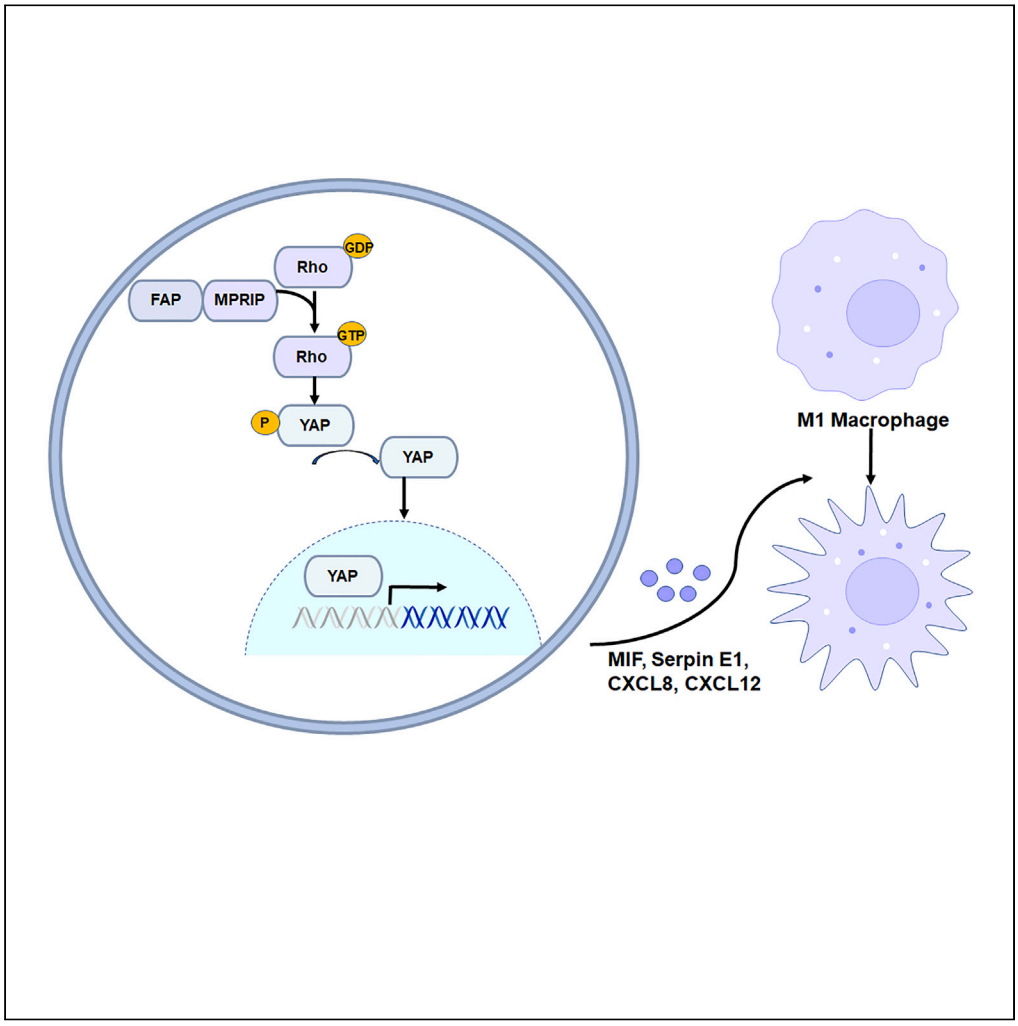

Dengbo Ji, Jinying Jia, Xinxin Cui, Zhaowei Li, Aiwen Wu

wuaw@sina.com

Highlights

FAP was upregulated in MC patients and negatively correlated with prognosis

FAP promoted CRC cell growth, invasion and metastasis, and enhanced chemoresistance

FAP regulated the Rho/Hippo/YAP signaling pathway

FAP induced TAM recruitment and M2 polarization

Ji et al., iScience 26, 106600
June 16, 2023
https://doi.org/10.1016/j.isci.2023.106600

iScience

CellPress
OPEN ACCESS

Article

FAP promotes metastasis and chemoresistance via regulating YAP1 and macrophages in mucinous colorectal adenocarcinoma

Dengbo Ji,[1,2] Jinying Jia,[1,2] Xinxin Cui,[1] Zhaowei Li,[1] and Aiwen Wu[1,3,*]

SUMMARY

Mucinous colorectal adenocarcinoma (MC) is less likely to respond to chemotherapy and is associated with poorer prognosis compared with non-MC (NMC). Fibroblast activation protein (FAP) was found and validated to be upregulated in MC patients and was negatively correlated with prognosis and therapeutic outcomes in colorectal cancer (CRC) patients who were treated with adjuvant chemotherapy. Overexpression of FAP promoted CRC cell growth, invasion and metastasis, and enhanced chemoresistance. Myosin phosphatase Rho-interacting protein (MPRIP) was identified as a direct interacting protein of FAP. FAP may influence the efficiency of chemotherapy and prognosis by promoting the crucial functions of CRC and inducing tumor-associated macrophages (TAMs) recruitment and M2 polarization through regulating theRas Homolog Family Member/Hippo/Yes-associated protein (Rho/Hippo/YAP) signaling pathway. Knockdown of FAP could reverse tumorigenicity and chemoresistance in CRC cells. Thus, FAP may serve as a marker for prognosis and therapeutic outcome, as well as a potential therapeutic target to overcome chemoresistance in MC patients.

INTRODUCTION

Mucinous colorectal adenocarcinoma (MC) is a rare histological subtype of colorectal cancer (CRC), accounting for 10–20% of CRC patients. It is characterized by abundant mucinous components that comprise at least 50% of the tumor volume.[1] MCs are frequently observed in advanced stages at the time of diagnosis. Compared with non-MC (NMC), MCs have typically poorer responses to chemotherapy.[2] However, administration of adjuvant chemotherapy to patients with MC is based on the same standard guidelines as for CRC. Therefore, there is an urgent need to find special treatment for patients with MC.

Several previous studies reported that MC has a different molecular signature to adenocarcinoma colorectal cancer (AC), while the exact molecular aberrations for this pattern of disease progression have still remained elusive.[3] Various molecular aberrations have been described in patients with MC. KRAS, BRAF, and PIK3CA are more frequently mutated in MC compared with NMC, leading to constitutive activation of these pathways.[4–7] However, a common mucinous pathway has not been identified yet.

To identify MC-related genes, we, in the present study, compared MC and AC samples from The Cancer Genome Atlas (TCGA) database and found that fibroblast activation protein (FAP) was highly expressed and correlated with poor prognosis of MC. FAP is a type II integral membrane protein that belongs to the family of plasma membrane-bound serine proteases.[8] It was found to be expressed in fibroblasts in a variety of epithelial cancers, including CRC.[9–11] In the present study, its tumor-promoting function and molecular mechanism in MC were further characterized.

RESULTS

FAP was upregulated in MC, indicating poor prognosis

To identify MC-related genes, we compared MC and AC samples from TCGA database using gene set enrichment analysis (GSEA). These data consisted of 674 CRC patients, including 585 ACs and 89 MCs. A supervised method (significance analysis of microarrays; SAM) was initially used to identify a statistical significance ($p < 0.01$) in differentially expressed genes between the samples (Figure S1A). With performing

[1]Key Laboratory of Carcinogenesis and Translational Research, Ministry of Education, Department of Gastrointestinal Surgery III, Peking University Cancer Hospital & Institute, No. 52 Fucheng Road, Haidian District, Beijing 100142, China

[2]These authors are contributed equally

[3]Lead contact

*Correspondence: wuaw@sina.com

https://doi.org/10.1016/j.isci.2023.106600

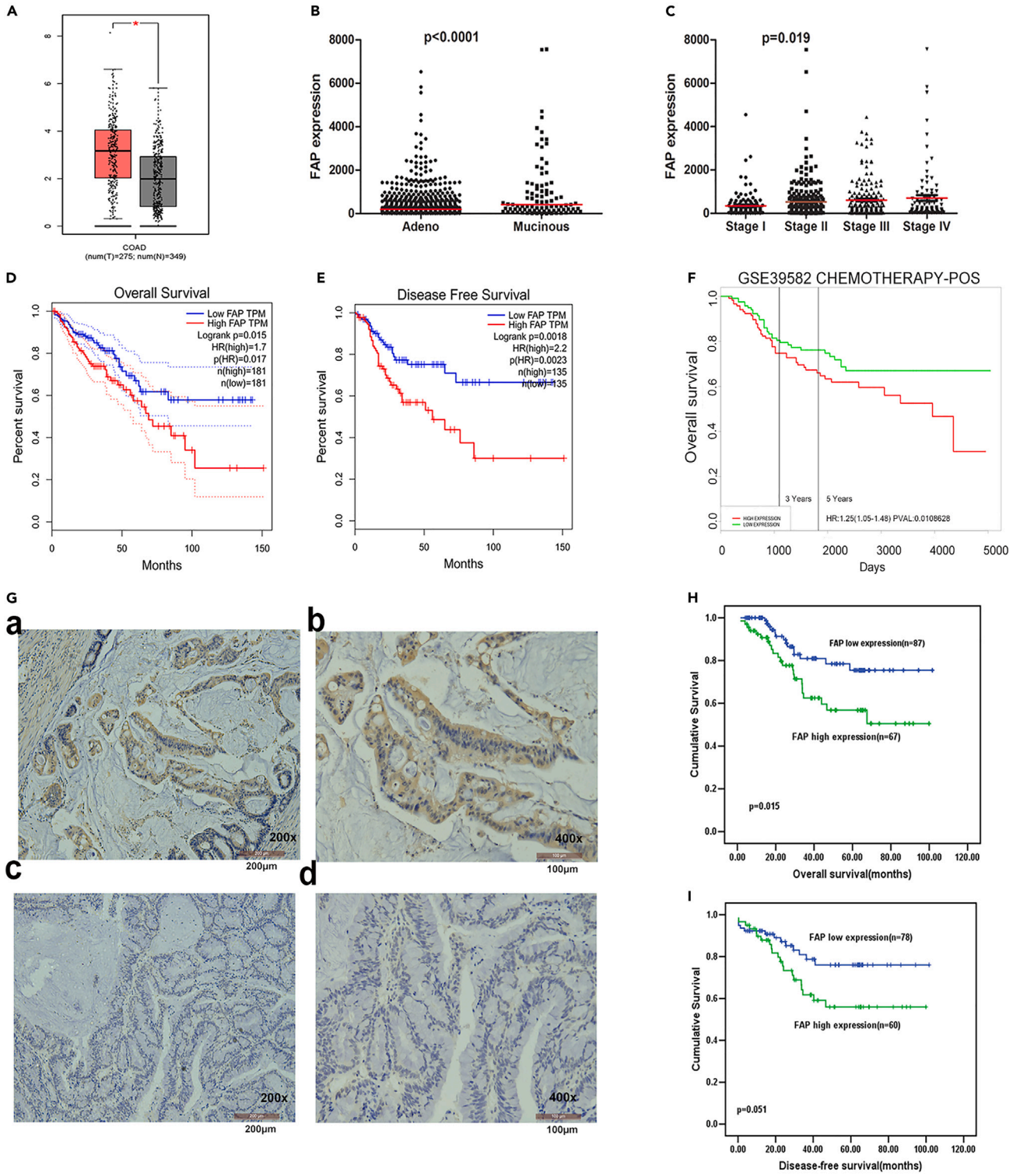

Figure 1. Association between FAP expression and prognosis with CRC

(A–E) from TCGA database. (A) The Expression level of FAP in CRC tissues and normal tissues from GEPIA website. The y axis is log-scale for log_2(TPM+1). Data are presented as means ± SEM, using Student's t test (* $p<0.05$).

(B) The expression level of FAP in MC and AC. The y axis shows the value scale for FPKM. The median value is shown with a red line, using Student's t test.

(C) The relationship between the expression level of FAP and advanced TNM stages. The median value is shown with a red line, using one-way ANOVA.

Figure 1. *Continued*

(D) Kaplan-Meier analysis of the correlation between expression level of FAP and OS or DFS (E) in patients with CRC, using the log rank test.

(F) Association of expression level of FAP with outcomes after chemotherapy in CRC patients from GSE39582, using the log rank test.

(G) Expression level of FAP in MC patients using IHC analysis. The positive staining of epithelium cells was expressed as brown, and the representative results are shown. (G-a-b) Strong positive expression in tumor epithelium cells; (G-c-d) negative expression in some colorectal cancer tissues. The length of scale bar of G-a and G-c is 200 μm; the length of scale bar of G-b and G-d is 100 μm.

(H) Kaplan-Meier analysis of the correlation between expression level of FAP and OS in MC patients, using the log rank test. (I) Kaplan-Meier analysis of the correlation between expression level of FAP and DFS in MC patients, using the log rank test. See also Figure S1.

univariate regression analysis of mRNA expression data, the mRNAs related to patients' overall survival (OS) and disease-free survival (DFS) ($p < 0.05$) were identified. Our findings showed that there was a significant increase in FAP expression in tumor tissues compared with matched adjacent normal tissues ($p < 0.05$, Figure 1A) using gene expression profiling and interactive analyses (GEPIA) website.[12] FAP was upregulated in MC compared with AC ($p < 0.0001$, Figure 1B). Increased expression level of FAP was noticeably correlated with advanced Tumor Node Metastasis (TNM) stages ($p = 0.019$, Figure 1C). Kaplan-Meier analysis revealed that patients with high expression level of FAP had shorter OS and DFS ($p = 0.015$ and 0.0018, respectively, log rank test; Figures 1D and 1E). The prognostic effect of FAP was validated in several GEO datasets (GSE17536, GSE39582, GSE28814, and GSE14333; Figures S1B–S1F).

We further analyzed associations between FAP expression and therapeutic outcomes in CRC patients who were treated with adjuvant chemotherapy in GSE39582 dataset. The chemotherapy regimens were primarily fluorouracil and folinic acid. For individuals who received adjuvant chemotherapy, high expression level of FAP was associated with a poor therapeutic outcome ($p = 0.0108$, the log rank test, Figure 1F).

We also utilized immunohistochemistry (IHC) to investigate the expression level of FAP in 188 MC tumors and corresponding non-tumor tissues. FAP was expressed not only on tumor cells but also on stromal cells. There was no significant correlation between FAP expression and gender, age at surgery, local tumor invasion (T stage), Lymph node metastasis (N stage), and M stage. FAP expression was associated with tumor location ($p = 0.048$) (Table S1). Increased expression level of FAP in tumor cells was significantly associated with a shorter OS and DFS ($p = 0.015$ and 0.051, respectively, Kaplan-Meier plot in Figures 1G–1I).

This suggests that the expression level of FAP is elevated in MC patients and is positively correlated with the malignancy of the tumor.

FAP promoted CRC cell proliferation *in vivo* and *in vitro*

In order to study the role of FAP in MC patients, LS174T and HCT8 cells were infected with FAP-overexpressing lentivirus to determine its effect on cell proliferation *in vitro* and *in vivo*. The expressions of FAP in LS174T, HCT8, and HCT116 cell lines were presented in Figure S2. Stable expression of FAP was confirmed by RT-qPCR and western blot (Figure 2A). Cell counting kit-8 (CCK-8) assay and clone formation assay showed that, in LS174T and HCT8 cell lines, upregulation of FAP promoted cell proliferation ($p < 0.05$; Figure 2B).

FAP-overexpressing cells and control cells were subcutaneously injected into BALB/c nude mice. Tumor growth in FAP overexpression was faster than that in the control group ($p < 0.05$). At the end of the experiment, the tumor weight of FAP-overexpression group was significantly increased ($p < 0.001$; Figure 2C). These results indicated that elevated expression level of FAP promotes the development of tumor *in vitro* and *in vivo*.

FAP promoted tumor invasion and liver metastasis

The effects of FAP on tumor invasion were assessed using the scratch wound-healing test and transwell assay. In FAP-overexpression group, LS174T cells markedly promoted than those in the control group in closing the wound at 24 h (Figure 3A). The ability of cell migration was significantly enhanced by overexpressing FAP as demonstrated in the Boyden chamber assay (Figure 3B). FAP also promoted HCT116 and HCT8 cells migration (Figures S2B–S2D).

Then, we constructed liver metastasis mouse model to study the function of FAP *in vivo*. LS174T cells with stably transfected luciferin (1×10^5 cells) were injected into the spleen subcapsular of nude mice. Tumor burden, as quantified by *in vivo* luminescence imaging, demonstrated promotion of liver tumor

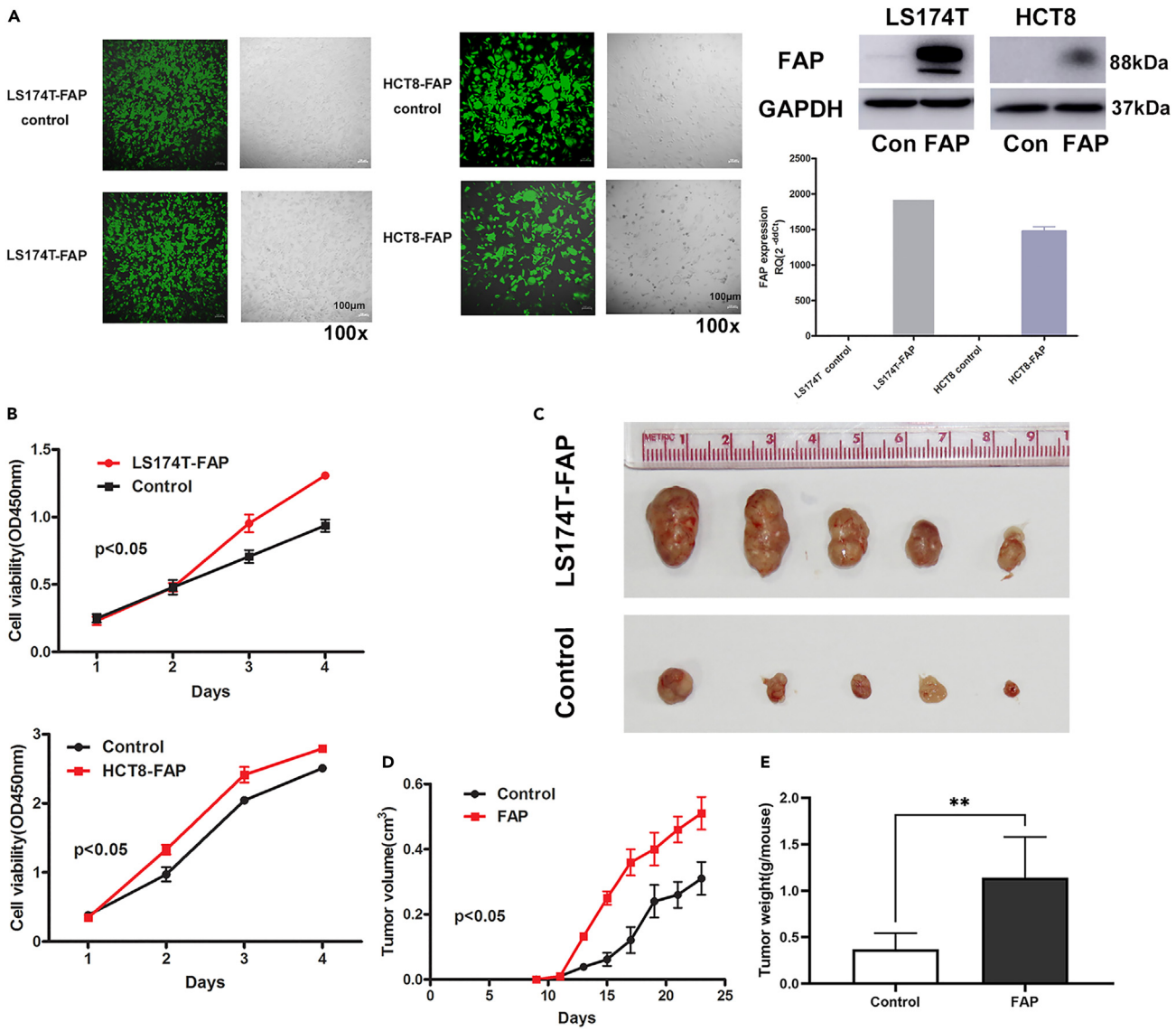

Figure 2. FAP promotes CRC cell growth *in vivo* and *in vitro*

(A) LS174T and HCT8 CRC cells were infected with FAP-overexpressing lentivirus; the length of scale bar is 100 μm. The expression level of FAP was assayed by quantitative RT-qPCR and western blot. Data are represented as mean ± SEM.

(B) Cell growth stimulated by FAP in LS174T and HCT8 CRC cells was detected by CCK-8 assay. Data are represented as mean ± SEM, using two-way ANOVA.

(C) The effects of FAP on the growth of LS174T cells were evaluated in BALB/c-nu mice.

(D) Tumor growth curves. Points and bars represent the mean tumor volume ±SD (six mice in each group, using two-way ANOVA, $p < 0.05$).

(E) Tumor weight derived from LS174T overexpressing FAP and control cells. Data are represented as mean ± SD, using Student's t test, $^{**}p < 0.01$. See also Figure S2.

development in FAP-overexpression group. The fluorescence intensity of liver metastasis in the FAP-overexpression group significantly increased compared with that in the control group ($p < 0.05$, Figures 3C–3E).

FAP induced chemoresistance of human CRC cells

Compared with HCT8, LS174T cell line is more resistant to 5-Fu (5-fluorouracil) (39.14 vs. 10.79 μM) and more sensitive to doxorubicin (0.19 vs. 2.42 μM). For CPT-11 (Campto, irinotecan), the sensitivity of LS174T (13.44 μM) is similar with HCT8 (15.67 μM) and more sensitive than HCT116 (27.35 μM). We further investigated whether FAP expression regulates chemosensitivity of CRC cells. To address this question, we

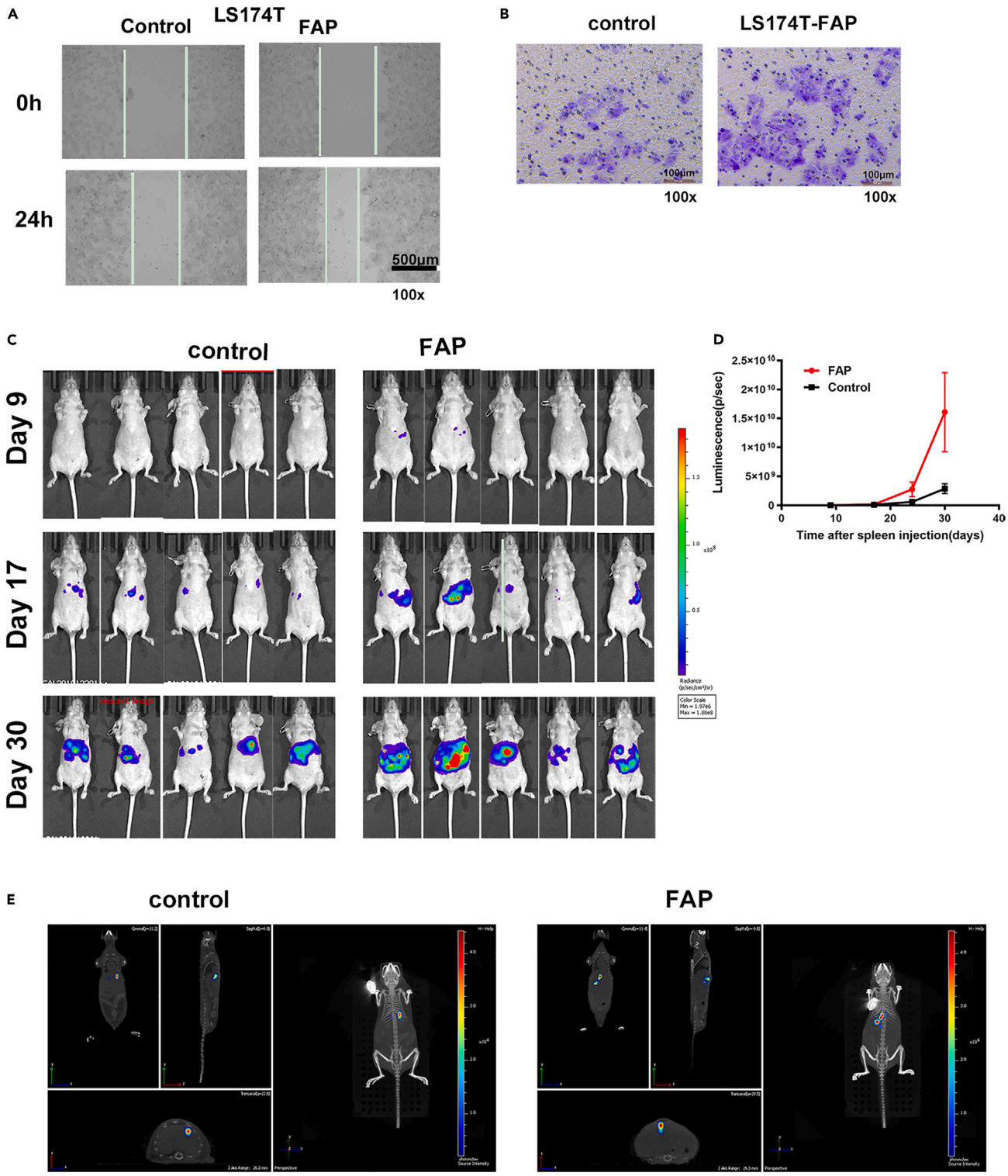

Figure 3. FAP promotes tumor invasion and liver metastasis

(A) Wound-healing assay showed that cell motility was enhanced following FAP overexpression in LS174T cells. Representative images from wounds made using a confluent monolayer of LS174T overexpressing FAP and control cells taken at 0 h and 24 h post wounding. The length of scale bar is 500 μm.

(B) The Boyden chamber assay was performed to investigate the effect of FAP on LS174T cells motility. The length of scale bar is 100 μm.

(C) FAP enhanced liver metastasis of LS174T cells. The tumor burden on liver was quantified by *in vivo* bioluminescence imaging using an IVIS Spectrum-CT.

Figure 3. *Continued*

(D) Tumor burden quantified weekly for LS174T overexpressing FAP, controls by *in vivo* bioluminescent imaging. Data are expressed as mean ± SD (n = 6). A mixed-effect linear model was used to determine significance of differences in tumor growth, $p < 0.05$.

(E) *In vivo* 3D bioluminescence imaging. See also Figure S2.

determined the half maximal inhibitory concentration (IC50) of 5-FU and CPT in control or FAP-overexpressing HCT8 and LS174T cells. A significant decrease was found in the chemosensitivity to 5-FU and CPT in HCT8 cells overexpressing FAP compared with control cells (5-Fu IC50: 35.51 vs. 10.79 μM, CPT IC50: 32.14 vs. 15.67 μM). These results were confirmed in LS174T cells (5-Fu IC50: 69.31 vs. 39.14 μM, CPT IC50: 56.87 vs. 13.44 μM) and HCT116 cells as well (CPT IC50: 48.26 vs. 27.35 μM). We also detected the sensitivity to doxorubicin and found that HCT8 and LS174T cells overexpressing FAP were more resistant than control cells (HCT8 cells, doxorubicin IC50: 3.85 vs. 2.42 μM; LS174T cells, doxorubicin IC50: 0.28 vs. 0.19 μM) (Figure 4A). We further compared FAP expression in 5-FU/CPT-sensitive/resistant HCT8 cell line pairs (HCT8/HCT8-5-FU/HCT8-CPT), which showed that FAP was highly expressed in HCT8-5-FU and HCT8-CPT cells (Figure 4B).

FAP expression affected tumor-initiating cell (TIC) phenotype

To validate that FAP is indeed involved in the regulation mechanism of TICs in CRC, we initially measured its expression in CRC spheroids using RT-qPCR and western blotting. HCT116 cells were cultured in the defined medium to obtain 3D spheroids. Culture and passage were then repeated until the development of third-generation spheroids. FAP was found to be remarkably upregulated in HCT116 spheroids compared with their counterparts (Figure 4C).

The self-renewal assay was used to assess a potential role for FAP in tumor initiation. It was unveiled that overexpression of FAP enhanced the spheroid-formation ability of CRC cells. Furthermore, single cells obtained from these FAP-overexpressing dissociated spheres could be clonally expanded and serially propagated, and daughter cells of FAP-overexpressing cells showed stronger sphere-formation capacity than the control cells, demonstrating that FAP promoted the self-renewal capability of CRC (Figure 4D).

We further investigated the effects of FAP on several cancer stem cell markers in CRC cells using RT-q-PCR and western blotting. It was noted that overexpression of FAP significantly induced expressions of BMI-1, MDR1, NANOG, ABCG2, and KLF4 (Figure 4E).

Myosin phosphatase Rho-interacting protein (MPRIP) could interact with FAP

To probe the FAP-associated pathways on an unbiased basis, we performed GSEA using high-throughput RNA-sequencing data of the TCGA database. FAP was shown to be associated with extracellular matrix organization and integrin cell surface pathways (Figure 5A). We then performed immunoprecipitation-mass spectrometry (IP-MS) proteomic analysis to identify proteins that interact with FAP. HCT8 cells stably expressing FAP were lysed and immunoprecipitated with an FAP antibody. The complexes were eluted and separated on 7.5% SDS-PAGE. Proteins in the gels were detected by silver staining, in-gel trypsin digested, and subjected to mass spectrometry (MS) analysis. From screening by MS, a series of proteins were identified as interacting specifically with FAP. Among them, MPRIP was identified from a specific band that originated the highest score and 31 unique peptides (Figure 5B). Co-immunoprecipitation analysis using lysates of HCT8 cells revealed that endogenous FAP interacts with MPRIP (Figure 5C). Furthermore, immunofluorescence analysis using confocal microscopy showed that FAP co-localizes with MPRIP in the cytoplasm. The above-mentioned results indicated that the FAP directly interacts with MPRIP (Figure 5D).

Regarding association between FAP and MPRIP, we explored the correlation between expression levels of FAP and MPRIP in CRC tissues using the university of Alabama at Birmingham cancer data analysis portal (UALCAN) website.[13] Our data revealed that expression level of MPRIP was positively correlated with FAP (Pearson's correlation coefficient = 0.59, $p < 0.001$) (Figure 5E). Therefore, the clinical significance of MPRIP in CRC was further analyzed. MPRIP was upregulated in MC compared with AC ($p < 0.0001$). Increased expression level of MPRIP was significantly correlated with advanced TNM stages and liver and nodal metastases (Figures 5F and 5G). Kaplan-Meier analysis revealed that patients with overexpression of MPRIP had shorter OS in TCGA dataset ($p = 0.0058$, Figure 5H) and GEO datasets (GSE17536, $p = 0.0329$; GSE41258, $p = 0.0031$ and GSE38832, $p = 0.046$; Figure S3). Increased expression level of MPRIP was

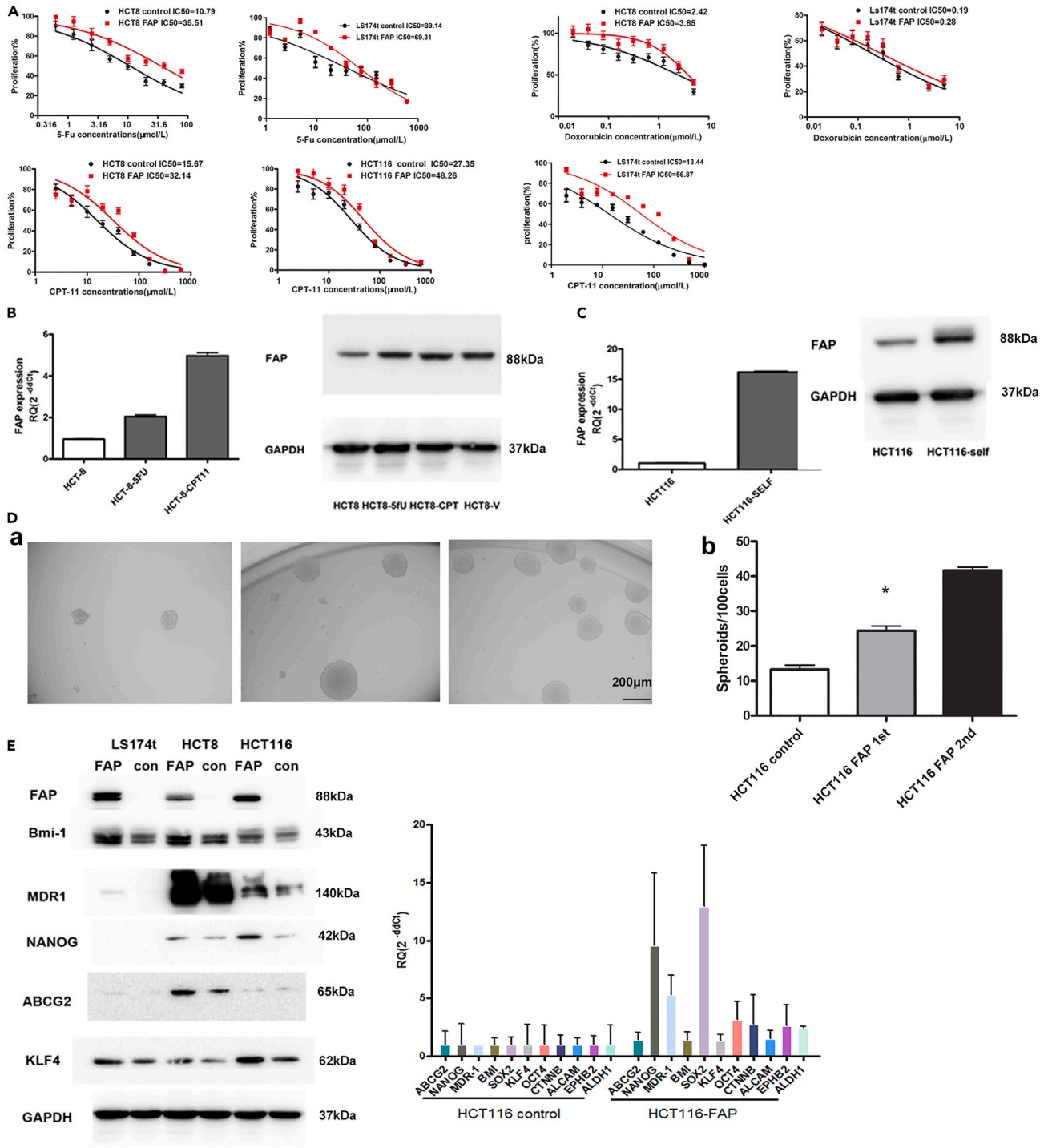

Figure 4. FAP induces chemotherapy resistance of CRC cells and drives the TIC phenotype

(A) The IC50 of 5-FU, CPT-11, and doxorubicin in control or FAP-overexpressing CRC cells, HCT8, HCT116, and LS174T. Data are represented as mean ± SEM.

(B) The expression level of FAP in HCT8, HCT8-5-Fu, and HCT8-CPT-11 cell lines was assayed by RT-qPCR and western blotting. Data are represented as mean ± SEM.

(C) The expression level of FAP in CRC spheroids was assayed using RT-qPCR and western blotting. Data are represented as mean ± SEM.

(D) (a) Phase-contrast micrographs illustrate that FAP-overexpressing HCT116 cells can form primary (first) and serially passaged (second) spheroids easily. The length of scale bar is 200 μm. (b) Histograms show spheroid-formation efficiency of the FAP-overexpressing cells and control cells. Bars are mean ± SD of three independent experiments (n = 3). Student's *t* test, *p <0.05.

(E) The expression levels of several stem cell markers in FAP-overexpressing HCT116 cells and control cells were assayed by RT-qPCR and western blotting. Data are represented as mean ± SEM.

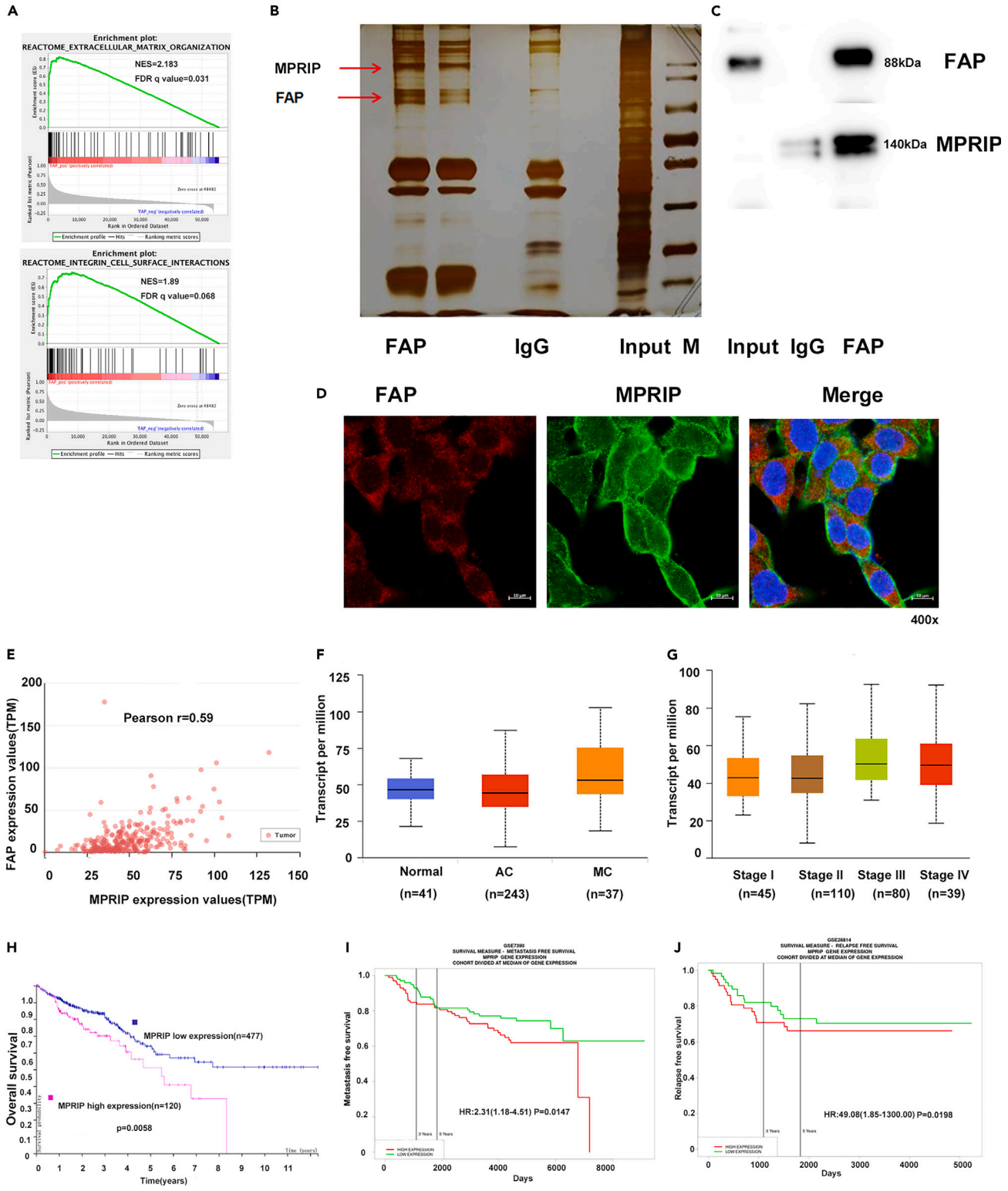

Figure 5. MPRIP interacted with FAP

(A) FAP was associated with extracellular matrix organization and integrin cell surface pathways in the GSEA of TCGA dataset.

(B) Silver staining was performed using the FAP-containing protein complex immunopurified from HCT8 cells stably expressing FAP on 7.5% SDS-PAGE.

(C) The interaction between FAP and MPRIP was detected by Co-IP assay.

Figure 5. *Continued*

(D) Confocal immunofluorescence microscopic images showed the co-localization of endogenous FAP (red) and MPRIP (green). DAPI was used to stain the nuclei (blue). The length of scale bar is 10 μm.

(E) Pearson's correlation analysis of expression levels of FAP and MPRIP from TCGA database.

(F) The expression level of MPRIP in normal tissues, MC, and AC. The box diagram shows the median, 25%, 75%, maximum, and minimum values , using Tukey's multiple comparison test.

(G) The relationship between expression level of MPRIP and advanced TNM stages. The box diagram shows the median, 25%, 75%, maximum, and minimum values, using Tukey's multiple comparison test.

(H) Kaplan-Meier analysis of the correlation between expression level of MPRIP and OS in CRC patients, using the log rank test.

(I) Kaplan-Meier analysis of the correlation between expression level of MPRIP and metastasis-free survival from GSE7390, using the log rank test.

(J) Kaplan-Meier analysis of the correlation between expression level of MPRIP and relapse-free survival from GSE28814, using the log rank test. See also Figure S3.

also noticeably correlated with CRC metastasis (GSE7390, $p = 0.0147$, Figure 5I) and relapse (GSE28814, $p = 0.0198$; GSE17536, $p = 0.0329$ and GSE14333, $p = 0.0001$; Figures 5J and S3).

FAP activated RhoA-Hippo signaling in CRC cells

MPRIP is a ubiquitously expressed protein that was previously identified as a direct RhoA binding partner by acting as a scaffold for multiple actin-remodeling proteins, such as RhoA and myosin phosphatase, and localizing them to actin filaments.

Small Rho guanosine triphosphatases (Rho GTPases) are key molecules in integrin signaling (32). In addition, the activity of Rho GTPases regulates the assembly of actin stress fibers and cell locomotion (33). Thus, we examined the effects of FAP on the activities of RhoA in CRC cells. Using a Rho GTPases pull-down assay, we observed that the FAP protein significantly enhanced the activity of RhoA in HCT116 cells (Figures 6A and 6B) and LS174T cells (Figure 6E).

Recently, the Hippo pathway was reported to be modulated by integrin-mediated changes in the actin cytoskeleton and Rho GTPase activity (34, 35). Therefore, we further investigated the effects of FAP on the Hippo pathway. Western blot analysis disclosed that FAP decreased YAP phosphorylation (Figure 6C). Immunofluorescence analysis using confocal microscopy showed that FAP significantly induced YAP nuclear translocation in HCT116 cells (Figure 6D). To investigate the functional correlation between FAP and MPRIP, we used MPRIP small interfering RNA (siRNA) to knock down the expression level of MPRIP in FAP-overexpressed LS174T cells. The expression of MPRIP was inhibited remarkably by MPRIP siRNA (Figure 6F). MPRIP siRNA significantly decreased the activity of RhoA in FAP-overexpressing LS174T cells (Figure 6F). We further investigate whether the effect of FAP on HIPP pathway depends on MPRIP. Western blot analysis disclosed that MPRIP knockdown rescued the level of YAP phosphorylation (Figure 6G). MPRIP siRNA inhibited cell proliferation in FAP-overexpressing LS174T cells assayed by the colony formation assay (Figure 6H). MPRIP siRNA inhibited cell motility in FAP-overexpressing LS174T cells assayed by wound-healing test (Figure 6I). The chemoresistance of LS174T cells induced by FAP was rescued by MPRIP siRNA (5-Fu IC50: 73.79 μM in control cells vs. 12.99 μM in MPRIP siRNA cells) (Figure 6J).

Taken together, by interacting with MPRIP, FAP-induced alterations, which include increased RhoA activity and activating Hippo pathway, likely contribute to the promotional effects of FAP on tumorigenicity and chemoresistance in CRC cells.

FAP induced the recruitment and polarization of tumor-associated macrophages (TAMs) cells

We next asked whether FAP overexpression affected the tumor microenvironment (TME). We first analyzed the correlation between infiltrating immune cells and FAP expression by using CIBERSORT[14] as an approach to dissect infiltration of specific immune cell subsets in the tumors from TCGA MCs data. The results showed that the fractions of $CD8^+$ T cells (4.8% vs. 7.5%) and $CD4^+$ memory resting T cells (14.6% vs. 18.5%) in the FAP-high-expression group were lower than those in the FAP-low-expression group ($p = 0.0013$, $p < 0.0001$). In the FAP-high-expression group, the fractions of macrophages M0 (26% vs.18%) and macrophages M2 (13% vs.7%) were higher than those in the FAP-low-expression group ($p < 0.0001$, $p = 0.0001$) (Figure 6K).

To quantify the effect of FAP on the recruitment and polarization of TAM cells, FAP-overexpressing cells and control cells were subcutaneously injected into BALB/c nude mice and the proportion of

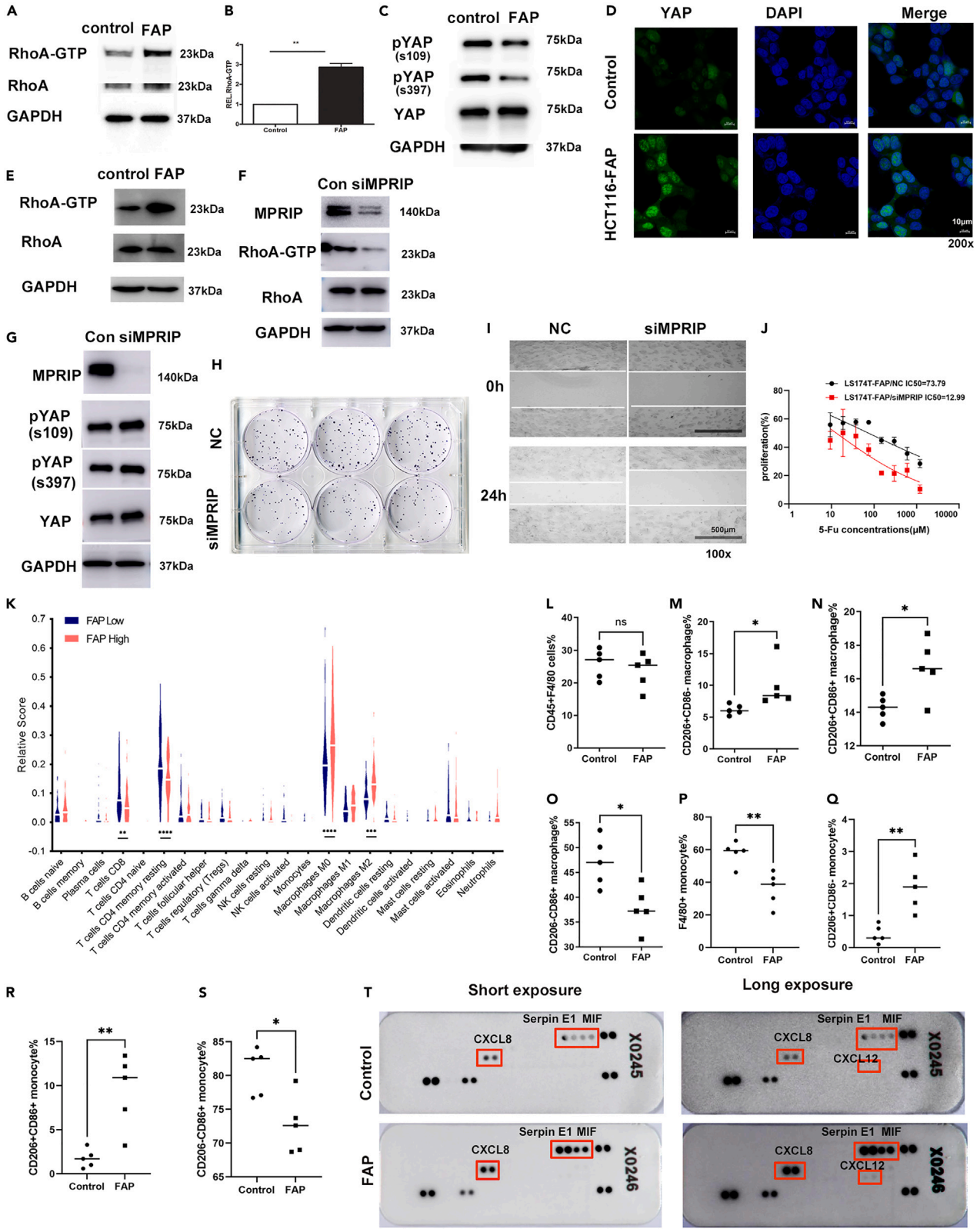
A
control FAP
RhoA-GTP 23kDa
RhoA 23kDa
GAPDH 37kDa
B
REL.RhoA-GTP
Control
FAP
C
control FAP
pYAP (s109) 75kDa
pYAP (s397) 75kDa
YAP 75kDa
GAPDH 37kDa
D
YAP
DAPI
Merge
Control
HCT116-FAP
10μm
200x
E
control FAP
RhoA-GTP 23kDa
RhoA 23kDa
GAPDH 37kDa
F
Con siMPRIP
MPRIP 140kDa
RhoA-GTP 23kDa
RhoA 23kDa
GAPDH 37kDa
G
Con siMPRIP
MPRIP 140kDa
pYAP (s109) 75kDa
pYAP (s397) 75kDa
YAP 75kDa
GAPDH 37kDa
H
NC
siMPRIP
I
NC
siMPRIP
0h
24h
500μm
100x
J
LS174T-FAP/NC IC50=73.79
LS174T-FAP/siMPRIP IC50=12.99
proliferation(%)
5-Fu concentrations(μM)
K
FAP Low
FAP High
Relative Score
B cells naive
B cells memory
Plasma cells
T cells CD8
T cells CD4 naive
T cells CD4 memory resting
T cells CD4 memory activated
T cells follicular helper
T cells regulatory (Tregs)
T cells gamma delta
NK cells resting
NK cells activated
Monocytes
Macrophages M0
Macrophages M1
Macrophages M2
Dendritic cells resting
Dendritic cells activated
Mast cells resting
Mast cells activated
Eosinophils
Neutrophils
L
CD45+F4/80 cells%
ns
Control
FAP
M
CD206+CD86- macrophage%
Control
FAP
N
CD206+CD86+ macrophage%
Control
FAP
O
CD206-CD86+ macrophage%
Control
FAP
P
F4/80+ monocyte%
Control
FAP
Q
CD206+CD86- monocyte%
Control
FAP
R
CD206+CD86+ monocyte%
Control
FAP
S
CD206-CD86+ monocyte%
Control
FAP
T
Short exposure
Long exposure
Control
FAP
Serpin E1
MIF
CXCL8
CXCL12
X0245
X0246

Figure 6. FAP activates RhoA-Hippo signaling in CRC cells. Knockdown of FAP reverses tumorigenicity and chemoresistance in CRC cells

(A) Analysis of active RhoA using RhoA-GTP pull-down assay in FAP-overexpressing HCT116 cells and control cells.

(B) RhoA expression in input samples was used as control for quantification and GAPDH as loading control (n = 2, two-sided Student's *t* test, ** p <0.01).

(C) Protein analysis of phosphorylated (S109, S397) and total YAP1 in FAP-overexpressing HCT116 cells and control cells.

(D) Immunofluorescence staining of YAP1 (green) in FAP-overexpressing HCT116 cells and control cells. DAPI was used to stain the nuclei (blue). The length of scale bar is 10 μm.

(E) Analysis of active RhoA using RhoA-GTP pull-down assay in FAP-overexpressing LS174T cells and control cells.

(F) The effect of siMPRIP on the activity of RhoA in FAP-overexpressing LS174T cells.

(G) Protein analysis of phosphorylated (S109, S397) and total YAP1 in MPRIP knock downed FAP-overexpressing LS174T cells and control cells.

(H) MPRIP siRNA inhibited cell proliferation in FAP-overexpressing LS174T cells assayed by the colony formation assay.

(I) MPRIP siRNA inhibited cell motility in FAP-overexpressing LS174T cells assayed by wound-healing test. The length of scale bar is 500 μm.

(J) MPRIP siRNA rescued the sensitivity to 5-Fu in FAP-overexpressing LS174T cells. Data are represented as mean ± SEM. (K) Fractions of immune cell subsets in tumor samples inferred from TCGA MCs data using CIBERSORT. Šídák's multiple comparisons test was used to compare the difference of immune cell subsets between FAP high- and low-expression groups, ** p <0.01, *** p <0.001, **** p <0.0001.

(L) Proportion of F4/80+ cells after gating on $CD45^+$ cell in tumor tissues from FAP-overexpressed and control groups.

(M) Proportion of CD206+$CD86^-$ macrophages in tumor.

(N) Proportion of CD206+$CD86^+$ macrophages in tumor.

(O) Proportion of CD206-$CD86^+$ macrophages in tumor.

(P) Proportion of F4/80+ cells after gating on $CD45^+$ cell in blood.

(Q) Proportion of CD206+$CD86^-$monocytes in blood.

(R) Proportion of CD206+$CD86^+$ monocytes in blood.

(S) Proportion of CD206-$CD86^+$ monocytes in blood. Student's *t* test was used to compare the difference of monocytes between FAP-overexpressed and control groups. *p < 0.05, **p < 0.01.

(T) Chemokine levels in conditioned medium (CM) from control or FAP-overexpressing LS174T cells measured by protein array. See also Figure S4.

M1/M2 macrophages in tumor tissues were assayed by flow cytometry analysis. In tumor tissues, FAP induced an increase in the percentage of CD206+CD86-/CD206+$CD86^+$ macrophages relative to the control group (p = 0.048, p = 0.018, respectively) (Figures 6M and 6N). A decrease in the percentage of CD206-$CD86^+$ macrophages was observed in FAP-overexpressed group (p = 0.0139) (Figure 6O). We also assayed the phenotypical alterations in circulating monocytes. Flow cytometry analysis showed that changes in circulating monocytes showed similar trends with macrophages in tumor tissues. A decrease in the percentage of F4/80+ monocytes was observed in FAP-overexpressed group (p = 0.0117) (Figure 6P). Compared with the control group, the percentages of CD206+$CD86^-$and CD206+$CD86^+$ monocytes increased in FAP-overexpressed group (p = 0.0031, p = 0.004, respectively) (Figures 6Q and 6R). The percentages of CD206-$CD86^+$ monocytes decreased in FAP-overexpressed group (p = 0.0117) (Figure 6S).

In order to further explore how FAP induced TAM recruitment and polarization, we used a protein array to measure a set of chemokines in conditioned medium (CM) of LS174T cells with or without ectopic FAP expression. The chemokines most significantly affected by FAP include MIF, Serpin E1/PAI-1, C-X-C motif chemokine ligand 8 and 12 (CXCL8 and CXCL12) (Figure 6T).

Knockdown of FAP reversed tumorigenicity and chemoresistance in CRC cells

To investigate the effects of suppression of FAP on the tumorigenic phenotype, we then used FAP siRNA to knock down the expression level of FAP in LS174T cells, which was confirmed by western blot (Figure 7A). The inhibition of FAP in LS174T cells remarkably decreased the cell proliferation (p = 0.022, two-way ANOVA, Figure 7B). A wound-healing assay revealed that the spreading of FAP siRNA-infected cells into the wound was noticeably slower than that of the control cells (Figure 7C). The inhibition of FAP also remarkably decreased the cell motility and invasion through matrigel, as demonstrated by the Boyden chamber assay (Figure 7D).

We further assessed whether suppression of FAP could modulate the chemoresistance of CRC cells. This was addressed by determining the IC50 of 5-FU in control or FAP-silenced CRC cells. In addition, we detected a significant decrease in the chemoresistance to 5-FU/CPT in the FAP-silenced LS174T cells compared with control cells (5-Fu IC50: 13.67 vs. 108.2 μM, p = 0.015; CPT IC50: 1.33 vs. 3.69 μM, p = 0.011) (two-way ANOVA, Figures 7E and 7F).

DISCUSSION

Compared with NMC, MC was more commonly diagnosed at an advanced stage of disease with a higher ratio of lymph node infiltration/peritoneal implant.[15] MC phenotype was reported to be an adverse

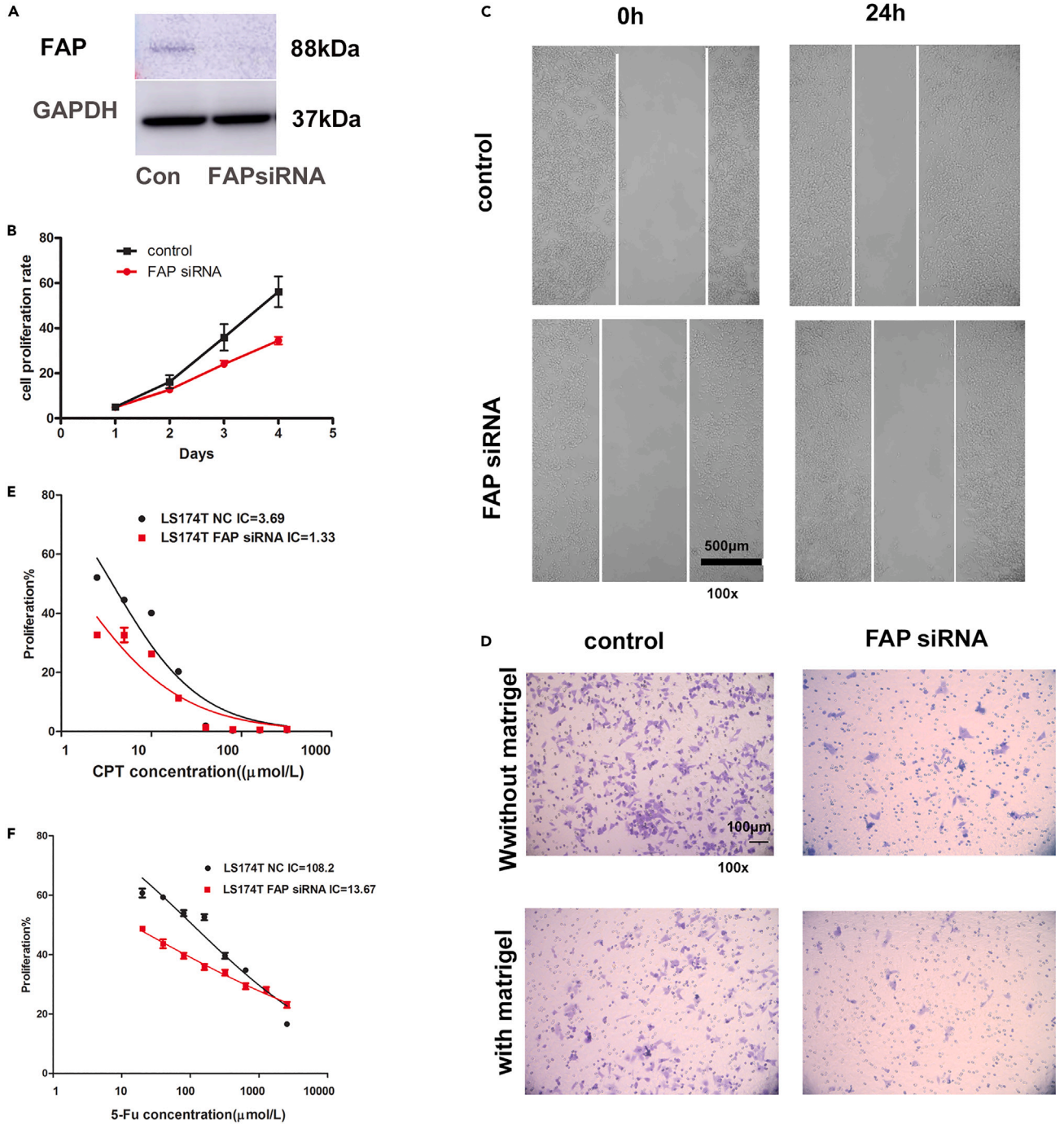

Figure 7. Knockdown of FAP reversed tumorigenicity and chemoresistance in CRC cells

(A) LS174T cells were transfected with FAP siRNA and control. The expression level of FAP was assayed by western blot.

(B) FAP siRNA inhibited cell growth in LS174T cells using CCK-8 assay. The results are expressed as mean ± SD of three independent experiments, using two-way ANOVA ($p < 0.05$).

(C) FAP siRNA inhibited cell motility. Wound-healing test was used to assay cell motility. The length of scale bar is 500 μm.

(D) The Boyden chamber assay was performed to assay cell migration and cell invasion. The length of scale bar is 100 μm.

(E) The IC50 of CPT-11 in FAP-knockdown LS174T cells and control cells. Data are represented as mean ± SEM, using two-way ANOVA.

(F) The IC50 of 5-FU in FAP-knockdown LS174T cells and control cells. Data are represented as mean ± SEM, using two-way ANOVA.

prognostic factor in CRC patients who underwent resection of liver metastases.[16,17] Several studies indicated a poor outcome in patients with MC who were treated with systemic chemotherapy despite different chemotherapy regimens being used in different trials.[18–21] MC might have a different molecular signature to AC for this pattern of disease progression and outcome. In the present study, we found that the expression level of FAP in MC was significantly higher than that in AC and was correlated with poor prognosis and resistance to chemotherapy. We further demonstrated that FAP enhances tumorigenicity of CRC by promoting tumor growth, metastasis, and chemoresistance *in vitro* and *in vivo*. We also found that FAP induced the recruitment and polarization of TAM M2.

Our study revealed that increased expression level of FAP was significantly correlated with advanced TNM stages and poor prognosis in CRC, consistent with previous studies, which supported FAP as an oncogenic factor. The expression level of FAP was reported to be correlated with higher grade, lymph node, and worse OS in gastric cancer,[22] glioma,[23] oral squamous cell carcinoma,[24] ovarian cancer,[25] and pancreatic ductal adenocarcinoma.[26] FAP, also called seprase, is a type II integral membrane protein belonging to the family of plasma membrane-bound serine proteases.[8] It was found to be expressed in fibroblasts in a variety of epithelial cancers, including CRC.[9–11] However, a number of scholars demonstrated that FAP expression is limited not only to stromal cells but also to some malignant epithelial cells. In the present study, we found that FAP was expressed on both tumor cells and stromal cells, which is consistent with previously conducted studies.[27,28] We, in the present study, for the first time, demonstrated that FAP expression in tumor cells was correlated with the poor prognosis in MC. We also found that FAP was negatively correlated with therapeutic outcome of CRC patients who underwent adjuvant chemotherapy.

We next investigated the effects of FAP on CRC development, progression, and sensitivity to chemotherapy by both *in vitro* and *in vivo* assays. Our results supported the hypothesis that FAP plays a substantial role during tumorigenesis and chemoresistance in CRC.

We then investigated the signaling pathways underlying FAP-mediated effects. Through GSEA analysis based on the TCGA database, FAP was shown to be associated with extracellular matrix organization and integrin cell surface pathways. We further identified MPRIP as an interacting protein with FAP by IP-MS analysis. MPRIP plays a critical role in actin cytoskeletal remodeling and is involved in cancer metastasis.[29] The current study demonstrated that high MPRIP expression is upregulated in MC and is associated with poor prognosis.

Small Rho GTPases are key molecules of integrin signal transduction.[30] In addition, the activity of Rho GTPases regulates the actin stress fiber assembly and cell movement.[31] Our data demonstrated that FAP functioned through interacting with MPRIP to activate RhoA and eventually drove the tumorigenic phenotype and chemotherapy resistance.

It was reported that the Hippo pathway is regulated by integrin-mediated changes in actin cytoskeleton and Rho GTPase activity.[32,33] Furthermore, we, in the present study, demonstrated that Hippo pathway was regulated by FAP-MPRIP/RhoA signaling cascades. Interaction of FAP with MPRIP led to activation of RhoA and dephosphorylation of YAP1, which induced nuclear localization of the protein.

The Hippo pathway has been shown to have a critical role in controlling organ size by regulating both cell proliferation and apoptosis. Components of the Hippo pathway were reported to be deregulated in various human malignancies, and expression levels of its major signal transducers were correlated with poor prognosis in CRC. Expression level of YAP1 in CRC patients was correlated with lymph node metastasis, liver metastases, and shorter OS.[34,35] In the intestine, inhibition of the activity of Hippo pathway results in stem cell expansion and neoplastic growth. YAP plays a pivotal role in maintaining stemness of stem cells and tissue homeostasis.[36,37] The current study demonstrated that FAP expression enhanced CRC tumor initiation. TICs, also known as tumor stem cells, are a rare tumor cell group, have the stem-like characteristics, and can undergo self-renewal and multiple differentiation.[38] Although few in number, they play a key role in drug resistance, metastasis, and cancer recurrence.[39] Studies have shown that tumor stem cells in CRC are associated with tumorigenicity, metastasis, and chemoresistance.[40,41] Chemotherapy can induce enrichment of tumor stem cells.[42] For example, oxaliplatin treatment of xenograft colon cancer cells showed an increase in CD133+ tumor cells.[43] These characteristics of stem cells may be related to multidrug resistance (MDR), cell cycle dormancy, decreased levels of reactive oxygen species (ROS), and DNA repair mechanisms.[44]

Recent studies have shown that YAP and TAZ in epithelial cells affect the TME and protect early tumors from immune surveillance. YAP activity controls the functionality of T regulatory cells (Tregs),[45] TAMs,[46] and myeloid-derived suppressor cells (MDSCs).[47] YAP activity regulates the expression of programmed death-ligand 1 (PD-L1).[48]

In our study, we found that the level of FAP expression was associated with immunosuppressive microenvironment. The high expression of FAP was positively correlated with the proportions of TAM M0 and M2 but negatively correlated with the infiltration of $CD8^+$ and $CD4^+$ memory resting T cells, indicating that FAP induced TAM recruitment and M2 polarization, which was confirmed by *in vivo* experiments. Macrophages are a major component of tumor-infiltrating lymphocytes that participate in innate and adaptive immunity. According to different conditions, macrophages can differentiate into the immune-activated macrophages (M1) with anti-tumor and pro-inflammatory functions or immunosuppressive phenotype macrophages (M2) with tumor-promoting function.[49]

In our study, FAP regulated protumourigenic chemokine including MIF, Serpin E1/PAI-1, CXCL8, and CXCL12. Previous studies have shown that MIF and Serpin E1/PAI-1 are strong chemoattractants that recruit TAMs and induce macrophage M2 polarization.[50–52] CXCL8 and CXCL12 are chemokines in CXC family that can regulate TAMs in tumors.[53] YAP and TEA Domain Transcription Factor 4 (TEAD4) could bind to the gene promoter of PAI-1 (SERPINE1) and regulate its expression and secretion.[54] YAP activation and translocation from cytoplasm to nucleus leads to YAP/p65 formation and binding to the nuclear factor κB (NF-κB) site, thereby enhancing interleukin-8 (IL-8)/CXCL8 expression.[55] Previous work has shown that NF-κB activity also increased the expression of CXCL12, thereby promoting tumor progression.[56] MIF expression could be regulated by AP-1 and NF-κB.[57] YAP/TAZ could induce the activation of AP-1, which then collaboratively regulates target genes expression with YAP/TAZ.[58]

The above-mentioned results indicated that FAP may suppress Hippo pathway by interacting MPRIP and activating Rho GTPase activity, leading to subsequent enhancement of TIC functions, the recruitment and polarization of M2 TAM cells. Taken together, our results indicated that FAP may influence the efficiency of chemotherapy and prognosis by promoting the crucial functions of CRCs through regulating the Rho/Hippo/YAP signaling pathway.

In conclusion, our results demonstrated that FAP could serve as a useful biomarker for prognosis and therapeutic outcome of MC, as well as a candidate therapeutic target to overcome chemoresistance by suppressing functions of CRC TICs, thereby improving therapeutic efficacy and survival in MC patients.

Limitations of the study

The expression of FAP was confined not only to stromal cells but also to some malignant epithelial cells. In this study, we found that FAP was expressed in both tumor cells and stromal cells, which was consistent with previous studies. In the present work, we just investigate the role of FAP in tumor cells. The effect of FAP expression in stromal cells on the prognosis of MC needs to be further studied. The correlation between FAP expression in stromal cells and tumor cells remains to be determined.

STAR★METHODS

Detailed methods are provided in the online version of this paper and include the following:

- KEY RESOURCES TABLE
- RESOURCE AVAILABILITY
  - Lead contact
  - Materials availability
  - Data and code availability
- EXPERIMENTAL MODEL AND SUBJECT DETAILS
  - Cell lines and experimental animals
  - Patients and collection of samples
- METHOD DETAILS
  - Study design
  - Oligonucleotide, lentiviral vector construction, and cell infection
  - Colony formation assay

- Cell cytotoxicity assay
- Spheroid formation assay
- *In vitro* cell growth, spreading, motility, and invasion assays
- *In vivo* mouse studies
- Western blot analysis
- Quantitative reverse transcription polymerase chain reaction (RT-qPCR)
- Immunoprecipitation (IP) and identification of proteins by liquid chromatography-tandem mass spectrometry (LC-MS/MS)
- Immunofluorescence staining
- Rho activation assay
- Immunohistochemistry (IHC)
- Flow cytometric analysis
- Cytokine array
- TCGA database
- Study approval

- QUANTIFICATION AND STATISTICAL ANALYSIS

SUPPLEMENTAL INFORMATION

Supplemental information can be found online at https://doi.org/10.1016/j.isci.2023.106600.

ACKNOWLEDGMENTS

This work was supported by the National Natural Science Foundation of China (81773214, 82173156). The authors would like to thank Dr. Bin Dong from Department of Pathology, Peking University Cancer Hospital & Institute, for her technical assistance.

AUTHOR CONTRIBUTIONS

Conceptualization, Project Administration: D.B.J. and A.W.W.; Supervision, Methodology, Writing – Review and Editing: D.B.J. and J.Y. J.; Writing – Original Draft, Data Curation, Software: D.B.J., X.X.C., Z.W.L., and A.W.W.; Formal Analysis, Data Curation: X.X.C. and Z.W.L.; Visualization, Resources, Validation, Investigation: J.Y.J., X.X.C., and Z.W.L.

DECLARATION OF INTERESTS

The authors have declared that no competing interest exists.

Received: June 18, 2022
Revised: February 16, 2023
Accepted: March 31, 2023
Published: April 8, 2023

REFERENCES

1. Bosman, F.T., Carneiro, F., Hruban, R.H., and Theise, N.D. (2010). WHO Classification of Tumours of the Digestive System, 4th edn (International Agency for Research on Cancer).

2. Kim, S.H., Shin, S.J., Lee, K.Y., Kim, H., Kim, T.I., Kang, D.R., Hur, H., Min, B.S., Kim, N.K., Chung, H.C., et al. (2013). Prognostic value of mucinous histology depends on microsatellite instability status in patients with stage III colon cancer treated with adjuvant FOLFOX chemotherapy: a retrospective cohort study. Ann. Surg Oncol. *20*, 3407–3413. https://doi.org/10.1245/s10434-013-3169-1.

3. Hanski, C. (1995). Is mucinous carcinoma of the colorectum a distinct genetic entity? Br. J. Cancer *72*, 1350–1356. https://doi.org/10.1038/bjc.1995.514.

4. Rosty, C., Young, J.P., Walsh, M.D., Clendenning, M., Walters, R.J., Pearson, S., Pavluk, E., Nagler, B., Pakenas, D., Jass, J.R., et al. (2013). Colorectal carcinomas with KRAS mutation are associated with distinctive morphological and molecular features. Mod. Pathol. *26*, 825–834. https://doi.org/10.1038/modpathol.2012.240.

5. Pai, R.K., Jayachandran, P., Koong, A.C., Chang, D.T., Kwok, S., Ma, L., Arber, D.A., Balise, R.R., Tubbs, R.R., Shadrach, B., and Pai, R.K. (2012). BRAF-mutated, microsatellite-stable adenocarcinoma of the proximal colon: an aggressive adenocarcinoma with poor survival, mucinous differentiation, and adverse morphologic features. Am. J. Surg. Pathol. *36*, 744–752. https://doi.org/10.1097/PAS.0b013e31824430d7.

6. Yokota, T., Ura, T., Shibata, N., Takahari, D., Shitara, K., Nomura, M., Kondo, C., Mizota, A., Utsunomiya, S., Muro, K., and Yatabe, Y. (2011). BRAF mutation is a powerful prognostic factor in advanced and recurrent colorectal cancer. Br. J. Cancer *104*, 856–862. https://doi.org/10.1038/bjc.2011.19.

7. Hugen, N., Simons, M., Halilović, A., van der Post, R.S., Bogers, A.J., Marijnissen-van Zanten, M.A., de Wilt, J.H., and Nagtegaal, I.D. (2015). The molecular background of mucinous carcinoma beyond MUC2. J. Pathol. Clin. Res. *1*, 3–17. https://doi.org/10.1002/cjp2.1.

8. Rettig, W.J., Su, S.L., Fortunato, S.R., Scanlan, M.J., Raj, B.K., Garin-Chesa, P., Healey, J.H., and Old, L.J. (1994). Fibroblast activation protein: purification, epitope mapping and induction by growth factors. Int. J. Cancer *58*, 385–392. https://doi.org/10.1002/ijc.2910580314.

9. Wikberg, M.L., Edin, S., Lundberg, I.V., Van Guelpen, B., Dahlin, A.M., Rutegård, J., Stenling, R., Oberg, A., and Palmqvist, R. (2013). High intratumoral expression of fibroblast activation protein (FAP) in colon cancer is associated with poorer patient prognosis. Tumour Biol. *34*, 1013–1020. https://doi.org/10.1007/s13277-012-0638-2.

10. Herrera, M., Herrera, A., Domínguez, G., Silva, J., García, V., García, J.M., Gómez, I., Soldevilla, B., Muñoz, C., Provencio, M., et al. (2013). Cancer-associated fibroblast and M2 macrophage markers together predict outcome in colorectal cancer patients. Cancer Sci. *104*, 437–444. https://doi.org/10.1111/cas.12096.

11. Henry, L.R., Lee, H.O., Lee, J.S., Klein-Szanto, A., Watts, P., Ross, E.A., Chen, W.T., and Cheng, J.D. (2007). Clinical implications of fibroblast activation protein in patients with colon cancer. Clin. Cancer Res. *13*, 1736–1741. https://doi.org/10.1158/1078-0432.CCR-06-1746.

12. Tang, Z., Li, C., Kang, B., Gao, G., Li, C., and Zhang, Z. (2017). GEPIA: a web server for cancer and normal gene expression profiling and interactive analyses. Nucleic Acids Res. *45*, W98–W102. https://doi.org/10.1093/nar/gkx247.

13. Chandrashekar, D.S., Karthikeyan, S.K., Korla, P.K., Patel, H., Shovon, A.R., Athar, M., Netto, G.J., Qin, Z.S., Kumar, S., Manne, U., et al. (2022). UALCAN: an update to the integrated cancer data analysis platform. Neoplasia *25*, 18–27. https://doi.org/10.1016/j.neo.2022.01.001.

14. Newman, A.M., Liu, C.L., Green, M.R., Gentles, A.J., Feng, W., Xu, Y., Hoang, C.D., Diehn, M., and Alizadeh, A.A. (2015). Robust enumeration of cell subsets from tissue expression profiles. Nat. Methods *12*, 453–457. https://doi.org/10.1038/nmeth.3337.

15. Nozoe, T., Anai, H., Nasu, S., and Sugimachi, K. (2000). Clinicopathological characteristics of mucinous carcinoma of the colon and rectum. J. Surg. Oncol. *75*, 103–107. https://doi.org/10.1002/1096-9098(200010)75:2<103::aid-jso6>3.0.co;2-c.

16. Viganò, L., Russolillo, N., Ferrero, A., De Rosa, G., Ferreri, E., Forchino, F., Sperti, E., and Capussotti, L. (2014). Resection of liver metastases from colorectal mucinous adenocarcinoma: is this a different disease? Results of a case-control study. Ann. Surg. *260*, 878–884. https://doi.org/10.1097/SLA.0000000000000981.

17. Lupinacci, R.M., Mello, E.S., Coelho, F.F., Kruger, J.A.P., Perini, M.V., Pinheiro, R.S., Fonseca, G.M., Cecconello, I., and Herman, P. (2014). Prognostic implication of mucinous histology in resected colorectal cancer liver metastases. Surgery *155*, 1062–1068. https://doi.org/10.1016/j.surg.2014.01.011.

18. Catalano, V., Loupakis, F., Graziano, F., Torresi, U., Bisonni, R., Mari, D., Fornaro, L., Baldelli, A.M., Giordani, P., Rossi, D., et al. (2009). Mucinous histology predicts for poor response rate and overall survival of patients with colorectal cancer and treated with first-line oxaliplatin- and/or irinotecan-based chemotherapy. Br. J. Cancer *100*, 881–887. https://doi.org/10.1038/sj.bjc.6604955.

19. Maisano, R., Azzarello, D., Maisano, M., Mafodda, A., Bottari, M., Egitto, G., and Nardi, M. (2012). Mucinous histology of colon cancer predicts poor outcomes with FOLFOX regimen in metastatic colon cancer. J. Chemother. *24*, 212–216. https://doi.org/10.1179/1973947812Y.0000000013.

20. Negri, F.V., Wotherspoon, A., Cunningham, D., Norman, A.R., Chong, G., and Ross, P.J. (2005). Mucinous histology predicts for reduced fluorouracil responsiveness and survival in advanced colorectal cancer. Ann. Oncol. *16*, 1305–1310. https://doi.org/10.1093/annonc/mdi244.

21. Mekenkamp, L.J.M., Heesterbeek, K.J., Koopman, M., Tol, J., Teerenstra, S., Venderbosch, S., Punt, C.J.A., and Nagtegaal, I.D. (2012). Mucinous adenocarcinomas: poor prognosis in metastatic colorectal cancer. Eur. J. Cancer *48*, 501–509. https://doi.org/10.1016/j.ejca.2011.12.004.

22. Miao, Z.F., Zhao, T.T., Wang, Z.N., Miao, F., Xu, Y.Y., Mao, X.Y., Gao, J., and Xu, H.M. (2014). Tumor-associated mesothelial cells are negative prognostic factors in gastric cancer and promote peritoneal dissemination of adherent gastric cancer cells by chemotaxis. Tumour Biol. *35*, 6105–6111. https://doi.org/10.1007/s13277-014-1808-1.

23. Busek, P., Balaziova, E., Matrasova, I., Hilser, M., Tomas, R., Syrucek, M., Zemanova, Z., Krepela, E., Belacek, J., and Sedo, A. (2016). Fibroblast activation protein alpha is expressed by transformed and stromal cells and is associated with mesenchymal features in glioblastoma. Tumour Biol. *37*, 13961–13971. https://doi.org/10.1007/s13277-016-5274-9.

24. Wang, H., Wu, Q., Liu, Z., Luo, X., Fan, Y., Liu, Y., Zhang, Y., Hua, S., Fu, Q., Zhao, M., et al. (2014). Downregulation of FAP suppresses cell proliferation and metastasis through PTEN/PI3K/AKT and Ras-ERK signaling in oral squamous cell carcinoma. Cell Death Dis. *5*, e1155. https://doi.org/10.1038/cddis.2014.122.

25. Mhawech-Fauceglia, P., Yan, L., Sharifian, M., Ren, X., Liu, S., Kim, G., Gayther, S.A., Pejovic, T., and Lawrenson, K. (2015). Stromal expression of fibroblast activation protein alpha (FAP) predicts platinum resistance and shorter recurrence in patients with epithelial ovarian cancer. Cancer Microenviron. *8*, 23–31. https://doi.org/10.1007/s12307-014-0153-7.

26. Lo, A., Li, C.P., Buza, E.L., Blomberg, R., Govindaraju, P., Avery, D., Monslow, J., Hsiao, M., and Puré, E. (2017). Fibroblast activation protein augments progression and metastasis of pancreatic ductal adenocarcinoma. JCI Insight *2*, e92232. https://doi.org/10.1172/jci.insight.92232.

27. Iwasa, S., Jin, X., Okada, K., Mitsumata, M., and Ooi, A. (2003). Increased expression of seprase, a membrane-type serine protease, is associated with lymph node metastasis in human colorectal cancer. Cancer Lett. *199*, 91–98. https://doi.org/10.1016/s0304-3835(03)00315-x.

28. Cao, F., Wang, S., Wang, H., and Tang, W. (2018). Fibroblast activation protein-alpha in tumor cells promotes colorectal cancer angiogenesis via the Akt and ERK signaling pathways. Mol. Med. Rep. *17*, 2593–2599. https://doi.org/10.3892/mmr.2017.8155.

29. Ono, R., Matsuoka, J., Yamatsuji, T., Naomoto, Y., Tanaka, N., Matsui, H., and Matsushita, M. (2008). M-RIP, a novel target of JNK signaling and a requirement for human cancer cell invasion. Int. J. Mol. Med. *22*, 199–203.

30. Takada, Y., Ye, X., and Simon, S. (2007). The integrins. Genome Biol. *8*, 215. https://doi.org/10.1186/gb-2007-8-5-215.

31. Nobes, C.D., and Hall, A. (1995). Rho, rac, and cdc42 GTPases regulate the assembly of multimolecular focal complexes associated with actin stress fibers, lamellipodia, and filopodia. Cell *81*, 53–62. https://doi.org/10.1016/0092-8674(95)90370-4.

32. Wang, L., Luo, J.Y., Li, B., Tian, X.Y., Chen, L.J., Huang, Y., Liu, J., Deng, D., Lau, C.W., Wan, S., et al. (2016). Integrin-YAP/TAZ-JNK cascade mediates atheroprotective effect of unidirectional shear flow. Nature *540*, 579–582. https://doi.org/10.1038/nature20602.

33. Dupont, S., Morsut, L., Aragona, M., Enzo, E., Giulitti, S., Cordenonsi, M., Zanconato, F., Le Digabel, J., Forcato, M., Bicciato, S., et al. (2011). Role of YAP/TAZ in mechanotransduction. Nature *474*, 179–183. https://doi.org/10.1038/nature10137.

34. Schlegelmilch, K., Mohseni, M., Kirak, O., Pruszak, J., Rodriguez, J.R., Zhou, D., Kreger, B.T., Vasioukhin, V., Avruch, J., Brummelkamp, T.R., and Camargo, F.D. (2011). Yap1 acts downstream of alpha-catenin to control epidermal proliferation. Cell *144*, 782–795. https://doi.org/10.1016/j.cell.2011.02.031.

35. Wang, Y., Xie, C., Li, Q., Xu, K., and Wang, E. (2013). Clinical and prognostic significance of Yes-associated protein in colorectal cancer. Tumour Biol. *34*, 2169–2174. https://doi.org/10.1007/s13277-013-0751-x.

36. Ramos, A., and Camargo, F.D. (2012). The Hippo signaling pathway and stem cell biology. Trends Cell Biol. *22*, 339–346. https://doi.org/10.1016/j.tcb.2012.04.006.

37. Barry, E.R., and Camargo, F.D. (2013). The Hippo superhighway: signaling crossroads converging on the Hippo/Yap pathway in stem cells and development. Curr. Opin. Cell Biol. *25*, 247–253. https://doi.org/10.1016/j.ceb.2012.12.006.

38. La Porta, C.A.M., and Zapperi, S. (2017). Complexity in cancer stem cells and tumor evolution: toward precision medicine. Semin. Cancer Biol. *44*, 3–9. https://doi.org/10.1016/j.semcancer.2017.02.007.

39. Kuşoğlu, A., and Biray Avcı, Ç. (2019). Cancer stem cells: a brief review of the current status. Gene *681*, 80–85. https://doi.org/10.1016/j.gene.2018.09.052.

40. O'Brien, C.A., Pollett, A., Gallinger, S., and Dick, J.E. (2007). A human colon cancer cell capable of initiating tumour growth in immunodeficient mice. Nature *445*, 106–110. https://doi.org/10.1038/nature05372.

41. Silva, V.R., Santos, L.d.S., Dias, R.B., Quadros, C.A., and Bezerra, D.P. (2021). Emerging agents that target signaling pathways to eradicate colorectal cancer stem cells. Cancer Commun. *41*, 1275–1313. https://doi.org/10.1002/cac2.12235.

42. Hu, X., Ghisolfi, L., Keates, A.C., Zhang, J., Xiang, S., Lee, D.K., and Li, C.J. (2012). Induction of cancer cell stemness by chemotherapy. Cell Cycle *11*, 2691–2698. https://doi.org/10.4161/cc.21021.

43. Das, P.K., Islam, F., and Lam, A.K. (2020). The roles of cancer stem cells and therapy resistance in colorectal carcinoma. Cells *9*. https://doi.org/10.3390/cells9061392.

44. Seebacher, N.A., Krchniakova, M., Stacy, A.E., Skoda, J., and Jansson, P.J. (2021). Tumour microenvironment stress promotes the development of drug resistance. Antioxidants *10*, 1801. https://doi.org/10.3390/antiox10111801.

45. Ni, X., Tao, J., Barbi, J., Chen, Q., Park, B.V., Li, Z., Zhang, N., Lebid, A., Ramaswamy, A., Wei, P., et al. (2018). YAP is essential for treg-mediated suppression of antitumor immunity. Cancer Discov. *8*, 1026–1043. https://doi.org/10.1158/2159-8290.CD-17-1124.

46. Orecchioni, M., Ghosheh, Y., Pramod, A.B., and Ley, K. (2019). Macrophage polarization: different gene signatures in M1(LPS+) vs. Classically and M2(LPS-) vs. Alternatively activated macrophages. Front. Immunol. *10*, 1084. https://doi.org/10.3389/fimmu.2019.01084.

47. Wang, G., Lu, X., Dey, P., Deng, P., Wu, C.C., Jiang, S., Fang, Z., Zhao, K., Konaparthi, R., Hua, S., et al. (2016). Targeting YAP-dependent MDSC infiltration impairs tumor progression. Cancer Discov. *6*, 80–95. https://doi.org/10.1158/2159-8290.CD-15-0224.

48. Yoo, G., Park, D., Kim, Y., and Chung, C. (2021). New insights into the clinical implications of yes-associated protein in lung cancer: roles in drug resistance, tumor immunity, autophagy, and organoid development. Cancers *13*, 3069. https://doi.org/10.3390/cancers13123069.

49. Ngambenjawong, C., Gustafson, H.H., and Pun, S.H. (2017). Progress in tumor-associated macrophage (TAM)-targeted therapeutics. Adv. Drug Deliv. Rev. *114*, 206–221. https://doi.org/10.1016/j.addr.2017.04.010.

50. Wang, L., Li, S., Luo, H., Lu, Q., and Yu, S. (2022). PCSK9 promotes the progression and metastasis of colon cancer cells through regulation of EMT and PI3K/AKT signaling in tumor cells and phenotypic polarization of macrophages. J. Exp. Clin. Cancer Res. *41*, 303. https://doi.org/10.1186/s13046-022-02477-0.

51. Martin-Manso, G., Galli, S., Ridnour, L.A., Tsokos, M., Wink, D.A., and Roberts, D.D. (2008). Thrombospondin 1 promotes tumor macrophage recruitment and enhances tumor cell cytotoxicity of differentiated U937 cells. Cancer Res. *68*, 7090–7099. https://doi.org/10.1158/0008-5472.CAN-08-0643.

52. Kubala, M.H., Punj, V., Placencio-Hickok, V.R., Fang, H., Fernandez, G.E., Sposto, R., and DeClerck, Y.A. (2018). Plasminogen activator inhibitor-1 promotes the recruitment and polarization of macrophages in cancer. Cell Rep. *25*, 2177–2191.e7. https://doi.org/10.1016/j.celrep.2018.10.082.

53. Qin, R., Ren, W., Ya, G., Wang, B., He, J., Ren, S., Jiang, L., and Zhao, S. (2022). Role of chemokines in the crosstalk between tumor and tumor-associated macrophages. Clin. Exp. Med. https://doi.org/10.1007/s10238-022-00888-z.

54. Marquard, S., Thomann, S., Weiler, S.M.E., Bissinger, M., Lutz, T., Sticht, C., Tóth, M., de la Torre, C., Gretz, N., Straub, B.K., et al. (2020). Yes-associated protein (YAP) induces a secretome phenotype and transcriptionally regulates plasminogen activator Inhibitor-1 (PAI-1) expression in hepatocarcinogenesis. Cell Commun. Signal. *18*, 166. https://doi.org/10.1186/s12964-020-00634-6.

55. Yuliani, F.S., Chen, J.Y., Cheng, W.H., Wen, H.C., Chen, B.C., and Lin, C.H. (2022). Thrombin induces IL-8/CXCL8 expression by DCLK1-dependent RhoA and YAP activation in human lung epithelial cells. J. Biomed. Sci. *29*, 95. https://doi.org/10.1186/s12929-022-00877-0.

56. Garg, B., Giri, B., Modi, S., Sethi, V., Castro, I., Umland, O., Ban, Y., Lavania, S., Dawra, R., Banerjee, S., et al. (2018). NFkappaB in pancreatic stellate cells reduces infiltration of tumors by cytotoxic T cells and killing of cancer cells, via up-regulation of CXCL12. Gastroenterology *155*, 880–891.e8. https://doi.org/10.1053/j.gastro.2018.05.051.

57. Osipyan, A., Chen, D., and Dekker, F.J. (2021). Epigenetic regulation in macrophage migration inhibitory factor (MIF)-mediated signaling in cancer and inflammation. Drug Discov. Today *26*, 1728–1734. https://doi.org/10.1016/j.drudis.2021.03.012.

58. Koo, J.H., Plouffe, S.W., Meng, Z., Lee, D.H., Yang, D., Lim, D.S., Wang, C.Y., and Guan, K.L. (2020). Induction of AP-1 by YAP/TAZ contributes to cell proliferation and organ growth. Genes Dev. *34*, 72–86. https://doi.org/10.1101/gad.331546.119.

59. Tom, B.H., Rutzky, L.P., Jakstys, M.M., Oyasu, R., Kaye, C.I., and Kahan, B.D. (1976). Human colonic adenocarcinoma cells. I. Establishment and description of a new line. In Vitro *12*, 180–191. https://doi.org/10.1007/BF02796440.

60. Schultz, R.M., Woods, W.A., and Chirigos, M.A. (1975). Detection in colorectal carcinoma patients of antibody cytotoxic to established cell strains derived from carcinoma of the human colon and rectum. Int. J. Cancer *16*, 16–23. https://doi.org/10.1002/ijc.2910160104.

61. Howell, G.M., Humphrey, L.E., Awwad, R.A., Wang, D., Koterba, A., Periyasamy, B., Yang, J., Li, W., Willson, J.K., Ziober, B.L., et al. (1998). Aberrant regulation of transforming growth factor-alpha during the establishment of growth arrest and quiescence of growth factor independent cells. J. Biol. Chem. *273*, 9214–9223. https://doi.org/10.1074/jbc.273.15.9214.

62. Kong, K.L., Kwong, D.L.W., Chan, T.H.M., Law, S.Y.K., Chen, L., Li, Y., Qin, Y.R., and Guan, X.Y. (2012). MicroRNA-375 inhibits tumour growth and metastasis in oesophageal squamous cell carcinoma through repressing insulin-like growth factor 1 receptor. Gut *61*, 33–42. https://doi.org/10.1136/gutjnl-2011-300178.

STAR★METHODS

KEY RESOURCES TABLE

REAGENT or RESOURCE	SOURCE	IDENTIFIER
Antibodies		
FAP	Abcam	ab207178; RRID: AB_2864720
BMI1	Abcam	ab126783; RRID: AB_11127730
ABCG2	Abcam	ab108312; RRID: AB_10861951
LMO7	Abcam	ab224113
MDR1	Cell Signaling Technology Inc	13342; RRID: AB_2631176
NANOG	Cell Signaling Technology Inc	4903; RRID: AB_10559205
MPRIP	Cell Signaling Technology Inc	14396; RRID: AB_2798472
YAP	Cell Signaling Technology Inc	14074; RRID: AB_2650491
pS397YAP	Cell Signaling Technology Inc	13619; RRID: AB_2650554
pS109YAP	Cell Signaling Technology Inc	46931; RRID: AB_2799315
KLF4	Cell Signaling Technology Inc	4038; RRID: AB_2265207
FAP	Santa Cruz Biotechnology	sc-65398; RRID: AB_831316
CD45	BD Biosciences	clone 30-F11; Cat# 557659, RRID: AB_396774
CD86	BD Biosciences	clone GL1; Cat# 560956, RRID: AB_10563076
CD206	BD Biosciences	clone MR5D3; Cat# 564668, RRID: AB_2738882
F4/80	BD Biosciences	clone T45-2342; 565410, RRID: AB_2687527
Bacterial and virus strains		
LV-GV249/FAP/GFP	GeneChem Co., Ltd	N/A
LV-GV249/GFP	GeneChem Co., Ltd	N/A
Biological samples		
Paraffin tissue section of CRC patients	Peking University Cancer Hospital & Institute	N/A
Critical commercial assays		
CCK-8	Dojido	CK04
Bio-Rad SureBeads™ Magnetic Beads Kit	Bio-Rad	1614916
RhoA activation assay kit	Cytoskeleton	BK036
murine tumor dissociation kit	Miltenyi Biotec	130-095-929
Proteome Profiler Human Cytokine Array kit	R&D Systems, Inc.	ARY005B
Experimental models: Cell lines		
HCT116	ATCC	CCL-247
HCT8	ATCC	CCL-244
LS174T	ATCC	CL-188
Experimental models: mouse		
BALB/c-nu mice	Beijing HFK Bio-technology Co. Ltd	N/A
Oligonucleotides		
GAPDH forward 5′- TGCACCACCAACTGCTTAGC-3′	Invitrogen	N/A
GAPDH reverse 5′- GGCATGGACTGTGGTCATGAG-3′¢	Invitrogen	N/A
FAP forward 5′- GGAAGTGCCTGTTCCAGCAATG -3′¢	Invitrogen	N/A
FAP reverse 5′- TGTCTGCCAGTCTTCCCTGAAG -3′¢	Invitrogen	N/A

(*Continued on next page*)

Continued

REAGENT or RESOURCE	SOURCE	IDENTIFIER
BMI1 forward 5′- AGCAGCAATGACTGTGATGC-3′	Invitrogen	N/A
BMI1 reverse 5′-CAGTCTCAGGTATCAACCAG-3′	Invitrogen	N/A
ABCG2 forward 5′-CCTGGTGCTCCATGAGGAGAC-3′	Invitrogen	N/A
ABCG2 reverse 5′-CAGACTCTGACCTTTTGCCAGG-3′	Invitrogen	N/A
SOX2 forward 5′-ACATGAACGGCTGGAGCAAC-3′	Invitrogen	N/A
SOX2 reverse 5′-AGGAAGAGGTAACCACAGGG-3′	Invitrogen	N/A
OCT4 forward 5′-GACAACAATGAAAATCTTCAGGAGA-3′	Invitrogen	N/A
OCT4 reverse 5′-CTGGCGCCGGTTACAGAACCA-3′	Invitrogen	N/A
NANOG forward 5′-TGCCTCACACGGAGACTGTC-3′	Invitrogen	N/A
NANOG reverse 5′-TGCTATTCTTCGGCCAGTTG-3′	Invitrogen	N/A
CTNNB forward 5′-TGATGGAGTTGGACATGGCC-3′	Invitrogen	N/A
CTNNB reverse 5′-CTCATACAGGACTTGGGAGG-3′	Invitrogen	N/A
KLF4 forward 5′-AAGCCAAAGAGGGGAAGAC-3′	Invitrogen	N/A
KLF4 reverse 5′-CATCTGAGCGGGCGAATTTC-3′	Invitrogen	N/A
MDR-1 forward 5′-GCCTGGCAGCTGGAAGACAAATAC-3′	Invitrogen	N/A
MDR-1 reverse 5′-ATGGCCAAAATCACAAGGGTTAGC-3′	Invitrogen	N/A
ABCG2 forward 5′-GGAGGCCTTGGGATACTTTGAA-3′	Invitrogen	N/A
ABCG2 reverse 5′-GAGCTATAGAGGCCTGGGGATTAC-3′	Invitrogen	N/A
ALDH1 forward 5′-CGGGAAAAGCAATCTGAAGAGGG-3′	Invitrogen	N/A
ALDH1 reverse 5′-GATGCGGCTATACAACACTGGC-3′	Invitrogen	N/A
ALCAM forward 5′-TCCAGAACACGATGAGGCAGAC-3′	Invitrogen	N/A
ALCAM reverse 5′-GTAGACGACACCAGCAACAAGG-3′	Invitrogen	N/A
EPHB2 forward 5′-CGCCATCTATGTCTTCCAGGTG-3′	Invitrogen	N/A
EPHB2 reverse 5′-GATGAGTGGCAACTTCTCCTGG-3′	Invitrogen	N/A
siFAP5′-GAACAATATCCTAGAACAA dTdT -3′	RiboBio Co. Ltd.	N/A
siMPRIP5′-GACGGTTCTTCATCCTTTA dTdT -3′	RiboBio Co. Ltd.	N/A
Software and algorithms		
GraphPad Prism 6.0 software	GraphPad Prism Software Inc.	https://www.graphpad.com/

RESOURCE AVAILABILITY

Lead contact

Further information and requests for resources and reagents should be directed to and will be fulfilled by the lead contact, Aiwen Wu(wuaw@sina.com).

Materials availability

This study did not generate new unique reagents and all materials in this study are commercially available.

Data and code availability

- Data: All the data reported in this study will be shared by the lead contact upon request. This paper analyzes existing, publicly available data. These accession numbers for the datasets are listed in the key resources table.
- Code: This study does not report any original code. Five CRC datasets were downloaded from the GEO datasets (GSE28814, GSE7390, GSE17536, GSE39582, and GSE14333).
- Any additional information required to reanalyze the data reported in this paper is available from the lead contact upon request.

EXPERIMENTAL MODEL AND SUBJECT DETAILS

Cell lines and experimental animals

Human CRC cell lines HCT116, HCT8, and LS174T were purchased from the American Type Culture Collection (ATCC; Manassas, VA, USA), and were cultured in Dulbecco's modified Eagle's medium (DMEM; Gibco, New York, NY, USA) containing 10% fetal bovine serum (FBS), 100 U/ml penicillin sodium, and 100 mg/ml streptomycin sulfate in a humidified atmosphere with 5% CO_2 at 37°C. The cell lines were tested and authenticated (STR [short tandem repeat]) profiling. LS174T cell line was from MC removed from a woman patient.[59] HCT8 cell line was derived from adenocarcinoma of the ileocecum from a male patient.[60] HCT116 cell line is poorly differentiated and highly tumorigenic colon adenocarcinoma from a male patient.[61] Chemo-resistant cells HCT8-5Fu and HCT8-CPT11 were established by stepwise exposure of HCT8 cells to increasing concentrations of 5-Fu or CPT11. Male BALB/c-nu mice (age, 4–6 weeks old) were purchased from Beijing HFK Bio-technology Co. Ltd. (Beijing, China). Mice were maintained in a specific pathogen-free barrier facility and used in accordance with the protocols approved by the Institutional Animal Care and Use Committee (IACUC) at the Peking University Cancer Hospital.

Patients and collection of samples

The study protocol was approved by the Ethics Committees of Peking University Cancer Hospital & Institute (Beijing, China), and conducted in accordance with the Declaration of Helsinki. All patients signed the written informed consent form prior to start of the study. Tissues consisting of MC and surrounding non-tumor tissues were obtained from 188 patients who underwent surgical resections from 2007 to 2018. These samples were paraffin-embedded for immunohistochemistry. All samples were collected from patients who didn't receive any preoperative chemotherapy or radiotherapy, and were verified to contain at least 80% tumor cells. Final cutoff date of follow-up was October, 2018. A summary of the clinical characteristics of these patients is shown in Table S2.

METHOD DETAILS

Study design

TCGA database was used to identify MC-related genes and to analyze the correlation between gene expression and prognosis. A cohort of 188 MC patients was used to assess the association of fibroblast activation protein (FAP) expression with prognosis by immunohistochemistry. Sample collection and usage was approved by the Ethics Review Committees of Peking University Cancer Hospital & Institute and in accordance with the Declaration of Helsinki. All patients were informed prior to the study and a consent form was signed by each participant. The details of patients' inclusion and exclusion criteria were described below.

Manipulation of FAP expression and its consequences in tumor growth and metastasis were demonstrated in various *in vitro* and *in vivo* models. Immunoprecipitation and liquid chromatography-tandem mass spectrometry (LC-MS/MS) were performed to identify proteins that interact with FAP. All animal experiments were performed following protocols approved by the Institutional Animal Care and Use Committee (IACUC) at the Peking University Cancer Hospital. In all experiments, animals were assigned to various experimental groups at random, but investigators were not blinded. For survival studies, sample sizes of 5–8 mice per group were used. *In vivo* studies were terminated either when the animals succumbed to death or when tumor burden reached a protocol-specified size of 1.5 cm in maximum dimension.

Oligonucleotide, lentiviral vector construction, and cell infection

The small interfering RNAs (siRNAs) targeting FAP and MPRIP were synthesized by RiboBio Co. Ltd. (Guangzhou, China). An unrelated sequence was used as a negative control (RiboBio Co. Ltd., Guangzhou, China). The sequence was FAP siRNA, 5′ GAACAATATCCTAGAACAA dTdT -3′(sense). The sequence was MPRIP siRNA, 5′GACGGTTCTTCATCCTTTA dTdT -3′(sense). Stable transfection overexpressing FAP was generated by lentiviral transduction using a GV492 vector (GeneChem Co., Ltd, Shanghai, China). A lentiviral vector expressing green fluorescent protein alone (LV-GFP) was used as a control. Transfection of oligonucleotides or lentivirus construction was performed using Lipofectamine 2000 reagent (Invitrogen, Carlsbad, CA, USA) according to the manufacturer's instructions. HCT-8, HCT116, and LS174T cells were infected with recombinant lentivirus-transducing units plus 8 μg/mL Polybrene (Sigma-Aldrich, St Louis, MO, USA).

Colony formation assay

The cells were seeded into 6-well plates (300 cells/well) and cultured for two weeks. Then the cells were fixed with 4% polyformaldehyde for 30 min, then stained with crystal violet for 30 min, and then washed with water.

Cell cytotoxicity assay

The cells were seeded into 96-well plates (density, 10^4 cells/well) and treated with serial dilutions of the agent, in triplicate. Cell viability was measured with a cell counting kit-8 (CCK-8) (Dojido, Kumamoto, Japan) assay 48 h after treatment with compound or 5-FU, CPT-11. The percentage of cell survival in treated samples was normalized with untreated controls. The half maximal inhibitory concentration (IC50) was calculated with GraphPad Prism 5.0 (GraphPad Prism Software Inc., San Diego, CA, USA).

Spheroid formation assay

Spheroid formation was carried out by seeding 100 cells/well into 96-well ultra-low attachment plates (Corning Life Sciences, Acton, MA, USA) in a serum-free DMEM/F12 medium (Invitrogen, Carlsbad, CA, USA), supplemented with B27 (1:50; Gibco, New York, NY, USA), 50 ng/mL basic fibroblast growth factor (bFGF), 50 ng/mL EGF (Invitrogen, Carlsbad, CA, USA), and 1% methylcellulose (Sigma-Aldrich, St Louis, MO, USA). Cells were incubated in an incubator with CO_2 for 2–3 weeks, and spheres were counted under a stereomicroscope (Olympus, Tokyo, Japan). After that, spheres were collected by gentle centrifugation, dissociated to single cells, and then cultured to generate spheres of the next generation.

In vitro cell growth, spreading, motility, and invasion assays

Cell growth was assessed using CCK-8 kit (Dojindo, Tokyo, Japan) according to the manufacturer's instructions. Cells were plated in 96-well plates (5,000 cells per well) and cultured. Five duplicates were set. Cell proliferation was measured at 24h, 48h, 72h and 96 h respectively. After CCK-8 reagent was added to the plate and incubated for 1h at 37°C, the optical density (OD) value was measured at 450 nm. Cell spreading was evaluated by wound healing assay. Cells were plated into 6-well plates and cultured until attached. Wound Maker was used to create precise and repeatable wounds in all wells of the 6-well plate. Wound closure was observed by taking time elapsed micro-photos at 0 and 24 h after scratching. Cell motility or invasion was measured using a Boyden chamber assay with or without Matrigel. The cells were seeded in the upper part of the chamber containing serum-free medium and the lower part containing 10% serum medium. After 24 h culture, the cells were fixed with 4% paraformaldehyde and stained with 0.1% crystal violet. Photographs of three randomly selected fields of the fixed cells were taken and cells were counted. Experiments were performed in triplicate and repeated three times independently. The assays were carried out as previously described.[62]

In vivo mouse studies

CRC cell line-derived xenograft mouse models were used to explore the activity of FAP *in vivo*. LS174T xenografts were established by subcutaneous injection of 5×10^5 cells in the right flank of BALB/c-nu mice.

For mouse models of CRC with liver metastasis, LS174T cells with stably transfected luciferin (1×10^5 cells) were injected into the spleen subcapsular of nude mice through an abdominal incision under sterile conditions. After injection, the spleen was returned gently back to abdominal cavity and homoeostasis was assured. The area was thoroughly irrigated with warm sterile water and the abdominal cavity was closed in appropriate layers.

Tumor volumes and mouse weight were measured every three days. Volume was calculated using the following formula: $L \times A \times B \times 0.52$, where L denotes the longest dimension, and A and B are long and short diameters of the largest coronal section, respectively.

The tumor burden on liver was quantified by *in vivo* bioluminescence imaging using an IVIS Spectrum-CT (PerkinElmer, Waltham, MA, USA). The *in vivo* bioluminescence intensity of liver metastases was measured weekly, and the whole liver was examined by *in vitro* fluorescence imaging at the end of the experiment. Data were analyzed using Living Image 4.0 software (Caliper Life Sciences, Waltham, MA, USA).

Western blot analysis

Total protein lysates extracted from samples were separated with 10% sodium dodecyl sulfate-polyacrylamide gel electrophoresis (SDS-PAGE), and transferred to a polyvinylidene fluoride (PVDF) membrane. The membrane was blocked with 3% bovine serum albumin BSA, followed by incubation with antibodies. The membrane was then incubated with secondary horseradish peroxidase (HRP)-conjugated goat anti-rabbit or anti-mouse antibody (Jackson ImmunoResearch Laboratories Inc., West Grove, PA, UAS), and visualized using Immobilon™ Western Chemiluminescent HRP substrate (Millipore, Burlington, MA, USA). Glyceraldehyde 3-phosphate dehydrogenase (GAPDH) was used as the loading control. The following primary antibodies were used: rabbit monoclonal anti-human FAP, BMI1, ABCG2, rabbit polyclonal anti-human LMO7, (ab207178, ab126783, ab108312; ab224113; Abcam, Cambridge, UK), rabbit monoclonal anti-human MDR1, NANOG, MPRIP, YAP, pS397YAP, rabbit polyclonal anti-human pS109YAP, KLF4, (13342, 4903, 14396, 14074,13619,46931, 4038; Cell Signaling Technology Inc., Danvers, MA, USA).

Quantitative reverse transcription polymerase chain reaction (RT-qPCR)

Total RNA was extracted using TRIzol reagent (Invitrogen, Carlsbad, CA, USA) according to the manufacturer's protocol. For mRNA detection, total RNA (2 μg) was used in 20 μL of reverse transcriptase reaction to synthesize cDNA by using Moloney murine leukemia virus-reverse transcriptase (MMLV-RT) for RT-qPCR (Invitrogen, Carlsbad, CA, USA), according to the manufacturer's instructions. RT-qPCR was undertaken using the above RT products with the SYBR Green PCR Master Mix (Toyobo Co. Ltd., Osaka, Japan) on an ABI7500 PCR machine. PCR cycling conditions were as follows: at 95°C for 1 min, 40 cycles of 95°C for 15 s, at 60°C for 15 s, and at 72°C for 45 s. Data were presented as relative quantification (RQ) to GAPDH based on $2^{-\Delta\Delta Ct}$ method. All primers are listed in.

Immunoprecipitation (IP) and identification of proteins by liquid chromatography-tandem mass spectrometry (LC-MS/MS)

IP and elution procedures were performed using a Bio-Rad SureBeads Magnetic Beads Kit (Bio-Rad cat. 1614916; Bio-Rad Laboratories Inc., Hercules, CA, USA), according to the manufacturer's protocols. In all experiments, 8 μg/200 μL of mAb in coupling buffer was used for crosslinking to magnetic beads. Eluates (20 μL) from the beads were transferred to 0.5 mL microfuge tube with 2 μL neutralization buffer from the kit, mixed, and stored in liquid nitrogen. Analysis of immunoprecipitated proteins was conducted based shotgun proteomics. The samples were separated by SDS-PAGE followed by silver staining. The bands were isolated, trypsin-digested, and identified by LC/MS/MS. The trypsin-digested samples were first filtered through a 0.22 μm micro-pore membrane, and then subjected to liquid chromatography coupled with an LTQ Velos pro mass spectrometer (Thermo Fisher Scientific, Waltham, MA, USA). The Captrap Peptide column (20 μL/min) was used to load the 1 Peptide solution (10 μL), and separation of the analytes was performed on an RP-C18AQ column (100 μm id × 15 cm; Michrom Bioresources Inc., Auburn, CA, USA), and set the oven temperature to 35°C. The electrospray voltage was equal to 1.8 kV.

Immunofluorescence staining

For the detection of the intracellular distribution of FAP, MPRIP, and YAP, cells (1×10^4 cells/well) were seeded into six-well glass-bottom plates, fixed in 4% paraformaldehyde for 15 min, and then permeabilized with 0.2% Triton X-100 (PBS) for 10 min. Nonspecific binding sites were blocked with 1% BSA in PBS for 1 h. Cells were treated with a primary antibody specific for FAP (sc-65398, Santa Cruz Biotechnology), MPRIP (14396, Cell Signaling Technology, Beverly, MA) or YAP(14074, Cell Signaling Technology, Beverly, MA) overnight at 4°C. Thereafter, the cells were incubated with Alexa Fluor647-goat anti-mouse IgG (H + L) and Alexa Fluor488-goat anti-rabbit IgG (H + L) (Jackson ImmunoResearch, 115-605-003, 111-545-003). Herein, 4′,6-diamidino-2-phenylindole (DAPI) (Beyotime Institute of Biotechnology, Shanghai, China) was used to stain nuclei before capturing images. The images were acquired using a confocal microscope (Zeiss, Oberkochen, Germany). The red fluorescence indicated FAP expression, the green fluorescence indicated MPRIP or YAP expression, and the blue fluorescence indicated the nuclei.

Rho activation assay

When RhoA is bound to GTP, its status is activated. The amount of GTP-RhoA was herein measured with a RhoA activation assay kit (Cytoskeleton, BK036). HCT8 overexpressing FAP and control cells were lysed and centrifuged at 13000 g for 10 min at 4 °C. Next, the pellet was discarded, and the supernatants were used for the following assays. After that, 10% of the supernatant was mixed directly with loading buffer, and the

leftover supernatant was mixed with beads conjugated with the Rho-binding domain of Rhotekin for 2 h at 4 °C. Then, the beads were washed twice with PBS.

Immunohistochemistry (IHC)

IHC was performed using anti-Human FAP monoclonal antibody (ab207178; Abcam, Cambridge, UK). All images were examined by two experienced pathologists independently. The immunoreactivity of the proteins detected was recorded through the intensity of staining, and the percentage of immunoreactive cells was as follows: tissues with no staining were rated as 0, with a faint or moderate staining to strong staining in <25% of cells rated as 1, strong staining in 25–50% of cells rated as 2, and strong staining in >50% of cells rated as 3.

Flow cytometric analysis

The tumor masses from mice were removed, minced and processed using a gentle MACS dissociator and a murine tumor dissociation kit (Miltenyi Biotec). The cell suspensions were filtered through 70 μm cell strainers and washed with PBS. Single-cell suspensions were counted and stained with CD45 (APC-Cy7, clone 30-F11), CD86 (BUV395, clone GL1), CD206 (Alexa Fluor 647, clone MR5D3), F4/80 (PE, clone T45-2342). All flow cytometric analyzes were performed using FACSAria II flow cytometer (BD Biosciences, San Jose, California, USA) and the data were processed using FlowJo software (Tree Star). Gating strategy was shown in online Figure S4.

Cytokine array

To investigate the effect of FAP on the cytokine secretion, we compared the differences in cytokine secretion between FAP overexpressed LS174T and control cells. FAP overexpressed LS174T and control cells were cultured from serum-supplemented to serum-free culture (CD CHO, Gibco) through sequential adaptation method. 700 μL of cell supernatant were collected for each sample and centrifuged to remove particles. The supernatant was analyzed with the Proteome Profiler Human Cytokine Array kit (cat. no. ARY005B; R&D Systems, Inc.) according to the manufacturer's protocol.

TCGA database

TCGA level 3 RNASeq data for CRC patients were downloaded, including 674 CRC samples on July 18, 2017.

Study approval

Sample collection and usage was approved by the Ethics Review Committees of Peking University Cancer Hospital & Institute and in accordance with the Declaration of Helsinki. All patients were informed prior to the study and a consent form was signed by each participant. All animal experiments were performed following protocols approved by the Institutional Animal Care and Use Committee (IACUC) at the Peking University Cancer Hospital.

QUANTIFICATION AND STATISTICAL ANALYSIS

Data were expressed as median values or as mean ± standard deviation (SD). Comparisons were performed using the nonparametric Mann-Whitney U test or Kruskal-Walis test for continuous variables. Student's *t* test or one-way ANOVA was used to compare the expression of FAP among different groups. Pearson's correlation coefficient was used to estimate the correlation between the expression of FAP and MPRIP in CRC tissues. two-way ANOVA was used to compare the proliferation difference between different groups. Tukey's multiple comparison test was used to compare the differences between multiple groups. Šídák's multiple comparisons test was used to compare the difference of the infiltration rate of immune cells between the high expression group and the low expression group of FAP. Student's *t* test was used to compare the difference of manocytes between FAP overexpressed and control groups. Survival curves were plotted using the Kaplan-Meier analysis, and the log rank test was utilized to examine significant differences. A mixed-effect linear model was used to determine significance of differences in tumor growth. Statistical analyses were undertaken using GraphPad Prism 6.0 software (GraphPad Prism Software Inc., San Diego, CA, USA). $p < 0.05$ was considered statistically significant.